

# A COMPUTATIONAL METHOD TO EXTRACT MACROSCOPIC VARIABLES AND THEIR DYNAMICS IN MULTISCALE SYSTEMS \*

GARY FROYLAND <sup>†</sup>, GEORG A. GOTTWALD <sup>‡</sup>, AND ANDY HAMMERLINDL <sup>§</sup>

**Abstract.** A systematic method to identify and extract the slow variables from a high-dimensional complex multiscale system is developed. The slow subspace is unravelled by employing the transfer operator and the Koopman operator the eigenfunctions of which are used to define a projection onto a slow subspace. The full system is then reformulated in terms of those slow variables, and we present an effective multiscale integrator, which allows for a large macro time step to propagate forward the slow variables. We illustrate our method with several examples and show how the reduced slow dynamics faithfully represents statistical features of the full dynamics which are not coordinate dependent.

**Key words.** multiscale systems, slow-fast systems, transfer operator, Koopman operator

**AMS subject classifications.** 37xx, 37Mxx, 65Pxx

**1. Introduction.** Devising efficient computational methods to simulate high-dimensional complex systems is of paramount importance to a wide range of scientific fields, from nanotechnology, biomolecular dynamics, and material science to climate science. The sheer dimensionality, often paired with the presence of a rich hierarchy of temporal scales and several metastable states, makes direct computational modelling over the whole range of temporal scales intractable. However, usually the most important information is carried by the slow and large scales. For example, for weather forecasts we want to resolve the large scale high and low pressure fields rather than the small scale fast oscillations of the stratification surfaces, and for climate prediction in a coupled ocean-atmosphere model we want to learn about the slow dynamics of the ocean which is constantly kicked by fast-evolving weather systems swirling over the oceans. How to extract the set of relevant variables and the associated relevant dynamics from a dynamical system is one of the most challenging problems in computational modelling.

The dynamics of large complex systems are complicated by their high dimensionality and by the possible existence of active entangled processes running on temporal scales varying by several orders of magnitude. This project aims to develop innovative mathematical theory and numerical algorithms to identify a set of reduced low-dimensional macroscopic coordinates, given only a set of observations, that best capture the long term behaviour of such complex systems. We will tackle this problem on a fundamental level as well as on the practical level of implementation, ready for use by modellers in their respective application areas.

Obstacles to achieving these aims are the high-dimensionality of the system and the presence of metastable states in the slow as well as the fast variables.

---

\*The project was funded by the Australian Research Council Grant DP120104514.

<sup>†</sup>School of Mathematics and Statistics, University of New South Wales, Australia (G.Froyland@unsw.edu.au).

<sup>‡</sup>School of Mathematics and Statistics, University of Sydney, Australia (georg.gottwald@sydney.edu.au).

<sup>§</sup>School of Mathematics and Statistics, University of Sydney, Australia and School of Mathematics and Statistics, University of New South Wales, Australia (ahammerlindl@gmail.com).

One of the main tools to overcome the curse of dimensionality in complex systems is dimension reduction, i.e. describing the effective dynamics of a high-dimensional dynamical system in terms of some essential variables, chosen in such a way that the collective effect of the unresolved variables is implicitly represented. There are two separate scenarios when such a dimension reduction is possible: scale separation and weak coupling [31]. Here we concentrate on the large class of time scale separated systems which include models from molecular dynamics, chemical kinetics and climate. Despite the obvious computational advantage of reducing the dimensionality, reductions of scale-separated systems offer the additional advantage that the time-step to be used in simulations can be orders of magnitudes larger since the reduced model only involves slow variables.

Given the importance and significance of this problem, a plethora of methods exists to perform dimension reduction [31]. For scale separated systems, averaging of deterministic and stochastic systems over the measure induced by the fast process has been used [1, 59]. In the case when the averaged dynamics turns out to be trivial, diffusive effects become important and singular stochastic perturbation theory (homogenization) can be employed [37, 40, 56, 45, 34, 57] to derive reduced equations for the slow variables, even if the underlying dynamics is deterministic (but sufficiently chaotic) [47, 33]. On short time scales, deterministic and stochastic center manifold theory [9, 7, 53, 54, 4, 58] is a well-known method to describe the dynamics locally close to a fixed point, in which the fast variables are slaved to the dynamics of the slow variables. A different approach [11, 10, 62, 34] uses the Mori-Zwanzig projection formalism [52, 65] in which the full deterministic equations including slow and fast variables are recast in a form which allows (in an uncontrolled fashion, however) the use of stochastic approximations.

Some of these methods have a rigorous mathematical footing with clearly stated assumptions for their validity [37, 40, 56, 9, 47, 33, 44]. However, from a practical view point these methods are limited to low-dimensional systems because they require the underlying equations to be known and to be of a simple enough form to allow for the required analytical manipulations.

In more complicated situations, i.e., in realistic applications, one has to resort to numerical simulations. There has been recent interest in the numerical simulation community in dimension reduction for scale-separated systems where the full large-dimensional system is so complicated that the analytical procedures of the methods above become impractical. We mention here the equation-free projection algorithms [30, 36] and the heterogeneous multiscale method [19, 20]. These methods have been applied to a wide range of problems, including modelling of water in nanotubes, micelle formation, chemical kinetics and climate modelling and data assimilation [45, 35, 51, 32].

There are, however, two severe shortcomings of these methods that prevent their applicability to general classes of multiscale dynamical systems. Firstly, all of the above methods assume that the slow variables are *explicitly known*. The identification of the slow variables, however, has so far been out of reach for systems involving long-lived transient states, so called metastable states, of the *slow* variables [12]. Secondly, the subsequent numerical evolution of the slow variables (in cases where they can be identified) is further complicated by the presence of *fast* metastable states.

Here we will tackle these two obstacles by developing transfer operator methods and methods involving its dual, the so called Koopman operator. Transfer and Koopman operators represent a complete global description of the dynamical system’s action on ensembles or observables and provide powerful tools for identifying global slow dynamical modes also known as strange eigenmodes, persistent patterns, metastable sets and almost-invariant sets [16, 17, 43, 50, 48, 49, 22]. Transfer operator methodologies have already been successfully used to detect and approximate slowly decaying modes in a variety of computationally demanding settings, including molecular dynamics, ocean dynamics, atmospheric dynamics, and general fluid flow [60, 26, 27].

The first question we address is: *What are the macroscopic variables?* In high-dimensional complex systems such as chemical reaction kinetics, the variables for which equations are formulated are not necessarily purely slow or fast. Moreover, the dynamics of the slow variables may involve transitions between several long-lived metastable states involving multiple slow time scales. This is a typical situation in climate dynamics [55], material science and molecular dynamics [18]. It is a non-trivial task to identify those slow variables, which may be functions of the full state space. Recently the diffusion map approach has been proposed [13, 12] to identify slow observables, which are functions of the variables. The reduction then consists of determining the temporal evolution of those functions. However, this approach fails in situations with slow metastable states, because each metastable state would be spuriously identified as a ‘slow variable’ [29]. This degeneracy renders the diffusion map impractical for such systems [12]. We propose a method that allows for a direct representation of the slow variables in the presence of slow metastable states. We will do so by extracting slow state variables utilizing the structure of the eigenfunctions of the transfer operator.

The second question we address is: *How can we efficiently evolve the macroscopic variables?* The general strategy underlying the current equation-free and the heterogeneous multiscale methods to propagate the slow dynamics is the following: Provided we know the relevant slow variables, the simulation is split between a macrosolver for the slow variables employing a large integration time-step and a microsolver, in which the full high dimensional system is integrated for a short burst employing a small integration time step. The underlying assumption is that the fast dynamics quickly relaxes to its equilibrium value (conditioned on the slow variables). (The two methods differ in the way the information of the microstep is utilized in the macrosolver to evolve the slow variables. Whereas the equation-free approach does this without any assumptions on the form of the reduced equations, using the output of the slow variables after the microstep, the heterogeneous multiscale methods estimate the vector field of the slow reduced equation employing averaging theorems for singularly perturbed Markov processes [37, 40, 56]). The effectiveness of short bursts to estimate averages is severely corrupted by the presence of fast metastable states. The presence of metastable states and the rare transitions between them severely impede the relaxation towards equilibrium [64], rendering short bursts ineffective to estimate the slow dynamics. Instead we will facilitate the estimation of averages by using the invariant density of the fast process as calculated efficiently from the transfer operator.

The paper is organised as follows. In Section 2 we present an abstract framework

for slow-fast systems. The basic concepts of the transfer and the Koopman operators are introduced in Section 3. Section 4 presents a novel algorithm to effectively detect the presence of a multiscale structure in a given dynamical system as well as identifying the possible slow degrees of freedom. The algorithm is illustrated with a suite of test problems. In Section 5 we present an algorithm to extract the reduced dynamics of the slow variables which were determined in Section 4. Here we use results from homogenization theory to fit parameters of a reduced stochastic differential equation (SDE) for the slow variables. Details on the computational issues involved in calculating the transfer operator and the Koopman operator are discussed in Section 6. We conclude with a discussion and an outlook in Section 7.

**2. An abstract framework for multiscale systems.** In model reduction it is common to consider a projection  $\mathcal{P} : \mathcal{Z} \rightarrow \mathcal{X}$ , where  $\mathcal{Z}$  represents the phase space of the full system, and  $\mathcal{X}$  is a lower-dimensional space where a reduced model of the dynamics captures its slowest scale behaviour; see for example [66, 31]. In this paper, we assume that we have no *a priori* knowledge about the map  $\mathcal{P} : \mathcal{Z} \rightarrow \mathcal{X}$ , only that it exists. In particular, we do not assume that we know what variables are slow or fast, respectively. Therefore, none of the techniques developed in this paper explicitly use the map  $\mathcal{P}$ , but rather exploit the structure it gives to the overall system.

For this, we assume that there is a dynamical system  $T : \mathcal{Z} \rightarrow \mathcal{Z}$  on the full space and a “reduced dynamics”  $S : \mathcal{X} \rightarrow \mathcal{X}$  such that the following properties hold:

1.  $S$  models the long-term behaviour of  $T$ ; that is, there is a large iterate  $N \gg 1$  such that  $\mathcal{P} \circ T^N \approx S \circ \mathcal{P}$ .
2. The short term behaviour of  $T$  can be approximated by dynamics on a fiber of  $\mathcal{P}$ . That is, if

$$z, T(z), \dots, T^n(z)$$

is an orbit of finite length  $n \ll N$ , then  $\mathcal{P}(T^i(z))$  is nearly constant for  $i = 0, \dots, n$  and there is a dynamical system  $\hat{T} : F \rightarrow F$  on the fiber  $F = \mathcal{P}^{-1}(\mathcal{P}(z))$  and the orbit

$$z, \hat{T}(z), \dots, \hat{T}^n(z)$$

of length  $n$  closely approximates that of  $T$ .

Figure 2.1 gives an illustration of this abstraction. For ease of exposition we restricted the presentation here to the case of deterministic systems with discrete time. In the general case, the full dynamics and/or the reduced dynamics could be continuous-time systems, and could have stochastic components, with the obvious modifications. For now, we only consider the case that  $T$  and  $S$  are discrete-time, deterministic systems.

To turn this abstraction into a fully rigorous definition, one could consider both the dynamical system  $T_\epsilon$  and the number  $N_\epsilon$  as depending on a parameter  $\epsilon > 0$ , such that, as  $\epsilon$  tends to zero,

$$N_\epsilon \rightarrow \infty, \quad \mathcal{P} \circ T_\epsilon^{N_\epsilon} \rightarrow S \circ \mathcal{P}, \quad \text{and} \quad T_\epsilon \rightarrow \hat{T}$$

under the appropriate notions of convergence. Indeed, such an approach is used in homogenization theory [31]. In this paper, we study numerical examples where  $\epsilon > 0$  is fixed, and so do not consider these convergence results in detail.

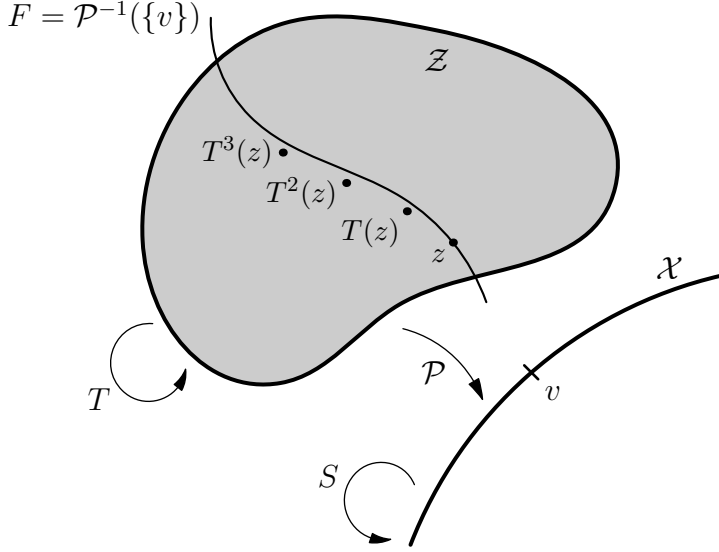


FIG. 2.1. An illustration of the abstract slow-fast framework. On short time scales, orbits of  $T$  stay close to fibers of  $\mathcal{P}$ . On long time scales, the orbits of  $T$ , after projecting by  $\mathcal{P}$ , can be approximated by orbits of  $S$ .

**3. The transfer and Koopman operator.** Information of the long-term behaviour of a dynamical system can often be obtained from spectral properties of linear operators associated with the dynamics. If  $T : \mathcal{Z} \rightarrow \mathcal{Z}$  represents a deterministic, discrete dynamical system, the transfer operator (or Perron-Frobenius operator)  $\mathcal{L}$  on  $L^2(\mathcal{Z})$  is defined by

$$(3.1) \quad \int g \cdot \mathcal{L}f \, dm = \int (g \circ T) \cdot f \, dm$$

for all  $f, g \in L^2(\mathcal{Z})$ . Unless otherwise noted, we take  $m$  to be Lebesgue measure on  $\mathcal{Z} \subset \mathbb{R}^d$ . If  $\mu$  is a measure defined by a density  $f$  (that is  $d\mu = f dm$ ), then  $\mathcal{L}f$  gives the resulting density after pushing the measure forward by  $T$ . A density  $f$  is invariant exactly when  $\mathcal{L}f = f$ . In other words,  $f$  is an eigenfunction with eigenvalue  $\lambda = 1$ . If this eigenvalue is simple, then  $f$  is the unique invariant density.

In certain settings, the transfer operator can be shown to be *quasi-compact*, meaning that (up to replacing  $\mathcal{L}$  by an iterate  $\mathcal{L}^n$ ) the operator can be decomposed as  $\mathcal{L} = F + V$  where  $F$  is a finite operator and  $V$  is contractive, that is,  $\|V\| < 1$  [3, 5, 6]. The spectrum of  $\mathcal{L}$  then contains a finite number of isolated eigenvalues  $\lambda_i$  satisfying  $|\lambda_i| > \|V\|$ . In particular, there is a gap in the spectrum between  $\lambda_1 = 1$  and  $\lambda_2$ , the next largest eigenvalue in magnitude. The magnitude of  $\lambda_2$  can be interpreted as the geometric rate at which non-equilibrium densities converge to the invariant density, often called the *rate of mixing*. In general, the leading eigenvalues  $\lambda_i$  with  $|\lambda_i|$  close to one correspond to the slowest decaying transients of the system. Rigorous results for computing this “outer spectrum” of eigenvalues can be found in [21, 5, 23].

A similar theory holds for the the adjoint of the transfer operator [50, 48, 49]. This is the Koopman operator  $\mathcal{K}$  defined simply by  $\mathcal{K}g = g \circ T$ .

In practice in this paper, we apply numerical schemes, which approximate  $\mathcal{L}$  and  $\mathcal{K}$  by finite dimensional operators. These approximations can be viewed as the transfer

and Koopman operators  $\tilde{\mathcal{L}}$  and  $\tilde{\mathcal{K}}$  now defined for a non-deterministic dynamical system  $\tilde{T}$  which adds local noise to the dynamics of  $T$ . The effect of this noise is to ensure that the images of the operators  $\tilde{\mathcal{L}}$  and  $\tilde{\mathcal{K}}$  are finite-dimensional, and so their eigenfunctions exist and can be computed. These operators can be defined in such a way that the dynamics of  $\tilde{T}$  closely resembles that of  $T$ , and the numerical implementation of these operators is described in detail in Section 6. Because of this, for the remainder of the paper we treat  $\mathcal{L}$  and  $\mathcal{K}$  as if they are compact operators on  $L^2(\mathcal{Z})$  and assume their leading eigenvalues and associated eigenfunctions can be calculated numerically.

**4. Identifying fast and slow coordinates.** We now consider the Koopman operator for a slow-fast system, and argue that its eigenfunctions can be used to find the projection  $\mathcal{P} : \mathcal{Z} \rightarrow \mathcal{X}$  without any *a priori* knowledge of the system.

**4.1. Defining fiber dynamics.** In the framework for slow-fast systems of Section 2, we can consider Koopman operators for both the full dynamics  $T$  with

$$\mathcal{K}_T g = g \circ T,$$

and the reduced dynamics  $S$  with

$$\mathcal{K}_S g = g \circ S.$$

Suppose that  $\psi : \mathcal{X} \rightarrow \mathbb{R}$  is an eigenfunction for the Koopman operator of the reduced dynamics  $\mathcal{K}_S$ . That is,  $\psi \circ S = \hat{\lambda} \psi$  with eigenvalue  $\hat{\lambda}$ . Then,

$$\psi \circ \mathcal{P} \circ T^N \approx \psi \circ S \circ \mathcal{P} = \hat{\lambda}(\psi \circ \mathcal{P})$$

so that  $\psi \circ \mathcal{P} : \mathcal{Z} \rightarrow \mathbb{R}$  approximately solves the eigenfunction equation  $\phi \circ T^N = \hat{\lambda} \phi$  for the Koopman operator of  $T^N$ . This suggests that  $\mathcal{K}_T$  has an eigenfunction  $\phi$  close to  $\psi \circ \mathcal{P}$  with eigenvalue  $\hat{\lambda}^{\frac{1}{N}}$ . As  $N \gg 1$ , this eigenvalue is very close to one.

On the other hand, if  $\phi : \mathcal{Z} \rightarrow \mathbb{R}$  is an eigenfunction of  $\mathcal{K}_T$  with eigenvalue  $\lambda$  such that  $0 < |\lambda| < 1$ , then as  $N$  is large, either  $\lambda^N$  is close to zero, or  $\lambda$  is very close to 1. In the latter case, for a finite orbit  $z, T(z), \dots, T^n(z)$  with  $n \ll N$  the values  $\phi \circ T^j(z) = \lambda^j \phi(z)$  are nearly constant. Since this orbit stays close to the fiber  $\mathcal{P}^{-1}(\{v\})$  and  $N$  is large, it suggests that  $\phi$  will be nearly constant along the fiber.

Suppose the Koopman operator associated with the full dynamics  $\mathcal{K}_T$  has a number of associated eigenfunctions  $\phi_i : \mathcal{Z} \rightarrow \mathbb{R}$  ( $i = 1, \dots, m$ ), all with eigenvalues close to one, then these give approximations of compositions  $\psi_i \circ \mathcal{P} : \mathcal{X} \rightarrow \mathbb{R}$ . If, further,  $\mathcal{X}$  can be identified with its image under the product map

$$\psi_1 \times \psi_2 \times \dots \times \psi_m : \mathcal{X} \rightarrow \mathbb{R}^m$$

then, the product

$$\phi_1 \times \phi_2 \times \dots \times \phi_m : \mathcal{Z} \rightarrow \mathbb{R}^m$$

gives an approximation of the mapping  $\mathcal{P} : \mathcal{Z} \rightarrow \mathcal{X}$ .

For simplicity, we restrict our study here to examples where the reduced space  $\mathcal{X}$  is one-dimensional. In this case the mapping  $\mathcal{P} : \mathcal{Z} \rightarrow \mathcal{X}$  can be well approximated by a single eigenfunction  $\phi : \mathcal{Z} \rightarrow \mathbb{R}$ . Extensions to higher-dimensional slow subspaces are discussed in Section 7. To see if an eigenfunction  $\phi$  is actually approximating

the (non-linear) projection  $P$  of a multiscale system, we develop a test for multiscale behaviour.

To do this, we first approximate the fast dynamics  $\hat{T} : F \rightarrow F$  defined on a fiber  $F := \mathcal{P}^{-1}(\{v\}) = \phi^{-1}(\{v\})$ . Assuming  $\phi$  is differentiable, its gradient  $\nabla\phi$  is a vector field on  $\mathcal{Z}$ . If this vector field is non-zero on a neighbourhood  $U$  of the fast fiber  $F$ , it defines a map  $\pi$  from  $U$  to  $F$  simply by flowing either along  $\nabla\phi$  or  $-\nabla\phi$  depending on whether the starting point  $z \in U$  satisfies  $\phi(z) < v$  or  $\phi(z) > v$ . Moreover, one can show by basic calculus that

$$\|\pi(z) - z\| \leq \frac{1}{C} \|\phi(\pi(z)) - \phi(z)\| = \frac{1}{C} \|v - \phi(z)\|$$

where  $C$  is the minimum value of  $\|\nabla\phi(z)\|$  on  $U$ . For a deterministic  $T$ , define  $\hat{T} : F \rightarrow F$  by  $\hat{T} = \pi \circ T$ . Then,

$$(4.1) \quad \|\hat{T}(z) - T(z)\| < \frac{1}{C} |v - \phi(T(z))| = \frac{1}{C} |v - \lambda\phi(z)| = \frac{1}{C} |1 - \lambda| |v|.$$

For  $\lambda$  close to one, the term  $|1 - \lambda|$  above will be close to zero, and  $\hat{T}$  will well approximate  $T$  and can be used to analyze the fast dynamics of the system. The closer to 1, the better the approximation for the dynamics  $\hat{T}$  on the fast fibers; therefore, in practice, we use the eigenfunction  $\phi$  which is associated with the second leading eigenvalue  $\lambda_2$ .

**4.2. Comparing eigenvalues.** To test for multiscale behaviour, we look at the Koopman operator for the fiber dynamics  $\hat{T}$ . The spectrum of the operator is connected to the rate of decay of correlations for the system [14]. Therefore, we expect for the fast dynamics that the spectrum does not have values as close to one, as for the spectrum of the full system.

In fact, we propose the following algorithm to test for multiscale behaviour:

**Algorithm 1**

1. Compute a numerical approximation  $\mathcal{K}$  of the Koopman operator of the full dynamical system  $T$ .
2. Determine its leading eigenvalues

$$\lambda_1, \lambda_2, \lambda_3, \dots$$

such that  $1 = |\lambda_1| \geq |\lambda_2| \geq |\lambda_3| \geq \dots$ .

3. Using the eigenfunction  $\phi$  associated to  $\lambda_2$ , take a fiber  $F = \phi^{-1}(\{v\})$  on which  $\|\nabla\phi\|$  is bounded away from zero.
4. Define the “fiber dynamics”  $\hat{T} : F \rightarrow F$  by  $\hat{T} = \pi \circ T$  where  $\pi$  is determined by the gradient flow.
5. Compute a numerical approximation  $\hat{\mathcal{K}}$  of the Koopman operator of the fiber dynamics  $\hat{T}$ .
6. Determine the leading eigenvalues of  $\hat{\mathcal{K}}$

$$\hat{\lambda}_1, \hat{\lambda}_2, \hat{\lambda}_3, \dots$$

7. Compare  $\hat{\lambda}_i$  to  $\lambda_i$ . A large ratio implies multiscale behaviour.

In a multiscale system, we expect the ratios to be large, roughly on the same order as the time-scale separation between the slow and fast dynamics, and in this paper we give examples where this is the case. See Table 4.1 for values computed for an example system which is introduced later in the paper.

If the same techniques are applied to a system without multiscale behaviour, then the simulated dynamics on a fiber will evolve at more-or-less the same rate as the full system. The resulting eigenvalues for the fiber dynamics may be smaller than for the full system, due to the fiber dynamics acting on a domain of smaller dimension, but the difference will be modest in nature. Specific examples of this are given in 4.3.1 and 4.3.3.

Once it is determined that a given dynamical system has multiscale behaviour and that  $\phi : \mathcal{Z} \rightarrow \mathbb{R}$  reasonably approximates the map  $\mathcal{P} : \mathcal{Z} \rightarrow \mathcal{X}$ , we know that  $\hat{T}$  defined on a fiber reasonably approximates the fast dynamics. It remains to give an approximation for the reduced slow dynamics  $S : \mathcal{X} \rightarrow \mathcal{X}$ . We describe such a construction in Section 5 and how it can be used to simulate the slow dynamics of the system for a time step much larger than is possible for the full dynamics.

In Algorithm 1, one must compute numerical approximations of Koopman operator and its eigenfunctions. In the examples in this paper, we use Ulam's method [63, 41] which approximates the transfer and Koopman operators by the dividing the space into a finite number of boxes. Care must be taken when applying Ulam's method to multiscale systems, and specific details about our implementation of the method are given in Section 6. Also, most of our example systems are defined by stochastic differential equations, and Section 6 also shows how the operators and their numerical approximations can be defined in this case.

One could also consider the eigenfunctions of the transfer operator defined with respect to the invariant measure. However, as discussed in Section 6 there are significant numerical problems in computing them to sufficient accuracy. Therefore, in this paper, we only consider eigenfunctions of the Koopman operator when computing level sets.

### 4.3. Examples.

**4.3.1. An analytic example.** Before delving into numerics, we first analyze an overly simple example which has known analytic formulas for the eigendecomposition. Consider two independent Ornstein-Uhlenbeck processes given by the SDE

$$(4.2) \quad dx_t = -x dt + dV_t$$

$$(4.3) \quad dy_t = -\frac{1}{\epsilon^2}y dt + \frac{1}{\epsilon} dW_t$$

for some fixed  $\epsilon > 0$  and where  $V_t$  and  $W_t$  are independent Wiener processes. If  $0 < \epsilon \ll 1$ , the  $y$ -variable evolves much faster than the  $x$ -variable and the SDE can be thought of as an example of a multiscale dynamical system where, in the abstract slow-fast framework of 2,  $\mathcal{P} : \mathcal{Z} \rightarrow \mathcal{X}$  is given by  $\mathcal{P}(x, y) = x$ .

For now, consider the  $x$  variable on its own. This is a classical one-dimensional Ornstein-Uhlenbeck system, and its spectral properties are known [61]. For each choice of flow time  $\tau$  there is an associated Koopman operator  $\mathcal{K}_\tau$  for the one-dimensional system given by (4.2). These form a semi-group of operators  $\mathcal{K}_\tau = e^{-\tau\mathcal{A}}$ , generated by an operator  $\mathcal{A}$ . Note the convention here that we include a minus sign when defining the generator, implying that eigenvalues of  $\mathcal{A}$  are non-negative. In the appropriate Hilbert space, the eigenfunctions of  $\mathcal{A}$  (and therefore each  $\mathcal{K}_\tau$ ) are the Hermite polynomials  $H_n$ . The eigenvalues of the infinitesimal generator  $\mathcal{A}$  are exactly the numbers  $\{0, 1, 2, \dots\}$  and  $\mathcal{A}H_n = nH_n$  for each  $n$ . To keep the analysis independent of the choice of flow-time  $\tau$ , we express all eigenvalues in terms of the generator  $\mathcal{A}$ .



The system in (4.3) is the same as that of (4.2), but with a rescaling of time by a factor of  $\epsilon^{-2}$ . Therefore, its generator has eigenvalues  $\{0, \epsilon^{-2}, 2\epsilon^{-2}, \dots\}$ .

For the two-dimensional system, as the two processes are independent, products of the form  $H_m \times H_n : \mathbb{R}^2 \rightarrow \mathbb{R}$ ,  $(x, y) \mapsto H_m(x) \cdot H_n(y)$  are eigenfunctions, and the eigenvalues for the full system are then of the form  $m + \epsilon^{-2}n$  for  $m, n \geq 0$ . Assuming  $\epsilon$  is sufficiently small, the leading eigenvalues, i.e., those with real part closest to zero, will be those with  $m$  small and  $n$  equal to zero. The function  $H_0$  is identically equal to one, and therefore  $(H_m \times H_0)(x, y) = H_m(x)$ .

The level sets of such a function are lines where the  $x$  value is constant, and the gradient  $\nabla(H_m \times H_0)$  points purely in the  $x$  direction. Therefore, one can verify that the fiber dynamics  $\hat{T} = \pi \circ T$  described in the last section corresponds exactly to leaving  $x$  constant and evolving  $y$  according to (4.3). That is, in this simple case, the fiber dynamics exactly captures the fast dynamics.

The leading eigenvalues associated to the fiber dynamics are (in terms of the generator)  $\{0, \epsilon^{-2}, \epsilon^{-2}, \dots\}$  which is exactly  $\epsilon^{-2}$  times the leading eigenvalues of the full system. Recall that  $\epsilon^{-2}$  is the difference in speed of the slow and fast systems.

In contrast, consider the same system, but with  $\epsilon$  equal to one. Then,  $x$  and  $y$  evolve under identical independent processes and one can check that the eigenspace associated to an eigenvalue  $\lambda = n$  is of dimension  $n + 1$ . In particular, for the second eigenvalue  $\lambda = 1$ , every eigenfunction  $\phi : \mathbb{R}^2 \rightarrow \mathbb{R}$  is in the span of  $H_1 \times H_0$  and  $H_0 \times H_1$  where  $H_1(x) = x$  and therefore  $\phi$  is of the form  $\phi(x, y) \mapsto (ax + by)$ . For  $\epsilon = 1$ , the system (4.2)–(4.3) is invariant under rotation about the origin, and so we can show that regardless of the exact values of  $a$  and  $b$ , the fiber dynamics are given by an Ornstein-Uhlenbeck process exactly as in (4.2). Hence, the eigenvalues associated to the fiber dynamics are  $\{0, 1, 2, \dots\}$ . The leading ten eigenvalues of the full system, are (when counted with multiplicity as they would be if calculated numerically)

$$0, 1, 1, 2, 2, 2, 3, 3, 3, 3$$

and the ratios are

$$\frac{0}{0}, \frac{1}{1}, \frac{2}{1}, \frac{3}{2}, \frac{4}{2}, \frac{5}{2}, \frac{6}{3}, \frac{7}{3}, \frac{8}{3}, \frac{9}{3}$$

These ratios are growing linearly, but are not large as in the slow-fast case. Ratios computed for a system with  $\epsilon \approx 1$  will be similar in magnitude.

**4.3.2. A skew-product example.** We now give an example system which exhibits metastable behaviour in both slow and fast variables, defined by the following SDE on  $\mathbb{R}^2$

$$(4.4) \quad dx = (x - x^3 + \frac{a}{\epsilon}y) dt$$

$$(4.5) \quad dy = \frac{1}{\epsilon^2}(y - y^3) dt + \frac{\sigma}{\epsilon} dW_t.$$

Here,  $W_t$  represents the standard Wiener process. Homogenization results (see [31, 57]) show that as  $\epsilon \rightarrow 0$ , the evolution of the  $x$  variable approaches that of a drift-diffusion process with the contribution of  $\frac{a}{\epsilon}y$  replaced by Gaussian noise. For numerical analysis, however, we only consider the system with the constants fixed at  $\epsilon = 0.01$ ,  $a = 0.02$ , and  $\sigma^2 = 0.113$ . For these parameters the fast  $y$  variable switches between states near  $y = -1$  and  $y = +1$  on the order of about 0.1 units of time. The slow  $x$  variable switches between states near  $x = -1$  and  $x = +1$  on the order of hundreds

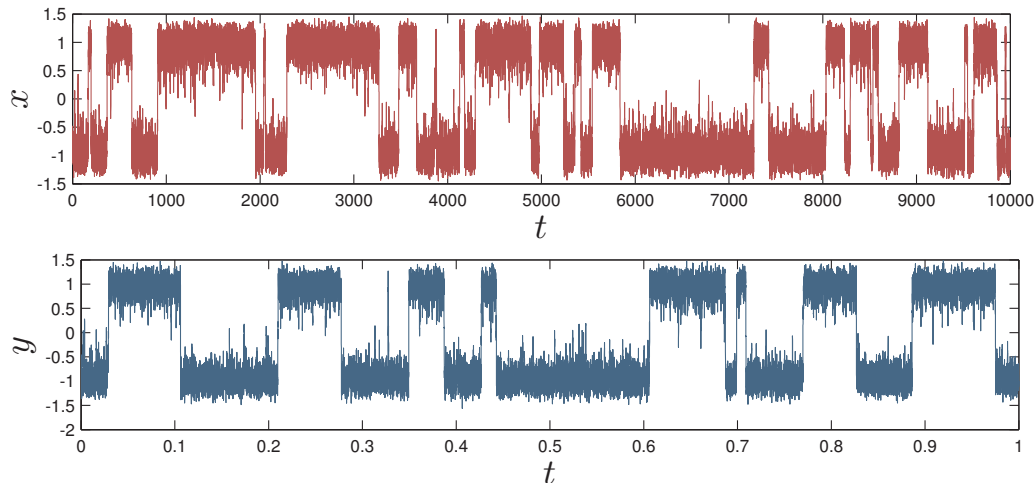


FIG. 4.1. The slow variable  $x$  and fast variable  $y$  computed for the system (4.4)–(4.5) with  $\epsilon = 0.01$ ,  $a = 0.02$ , and  $\sigma^2 = 0.113$ . The  $x$  variable is plotted over a total change of  $10^4$  units of time, while the  $y$  variable is plotted over a change of 1 unit of time.

of units of time, as illustrated in Figure 4.1. Because of the long time step needed to switch between them, we refer to these two states near  $x = \pm 1$  as the *slow metastable states* of the system.

For the algorithms developed here, the dynamical system is treated as a black box. It is represented by a computer routine which, given initial data  $z = (x, y) \in \mathbb{R}^2$ , returns a point  $T(z) \in \mathbb{R}^2$  given by the Euler-Maruyama integration method [38] after a single time step of  $\Delta t = 2 \times 10^{-6}$ . As the system is defined by a stochastic differential equation, calling the routine multiple times with the same input will yield different outputs.

The value  $\Delta t$  was chosen to be large enough to allow efficient computation of the system while being small enough to still simulate the fast dynamics of the system to an acceptable degree of accuracy.

To compute approximations of the eigenfunctions using Ulam’s method, we apply  $2 \times 10^4$  iterates of this time step  $\Delta t = 2 \times 10^{-6}$  for a total change in time of  $\tau = 0.04$ . Note that while this change in time corresponds to a large number of iterates, it is still much smaller than the time necessary for  $x$  to switch between its two metastable states. However, Ulam’s method computes accurate approximations of the eigenfunctions as shown in Figures 4.2 and 4.3.

We now choose a fiber and simulate dynamics restricted to that fiber as described in Algorithm 1. As will be explained in Section 6, a change in time of  $\hat{\tau} = 4 \times 10^{-5}$  is sufficient to accurately compute eigenvalues of the fiber dynamics. Note that this  $\hat{\tau}$  is much smaller than the time of  $\tau = 0.04$  used for the full dynamics.

The leading ten eigenvalues of both the full dynamics and the fiber dynamics are given in Table 4.1. For this example, a range of several values of  $v$  was used to compute dynamics on the fibers  $\phi^{-1}(\{v\})$  and gave similar eigenvalues. As these were computed using the different time steps  $\tau$  and  $\hat{\tau}$ , we also give the eigenvalues  $\chi_i$  for the infinitesimal generator, computed by taking  $\chi_i = -\frac{1}{\tau} \log(\lambda_i)$ . The final column gives the ratio  $\hat{\chi}_i/\chi_i$  of the eigenvalues of the two generators. These ratios are large

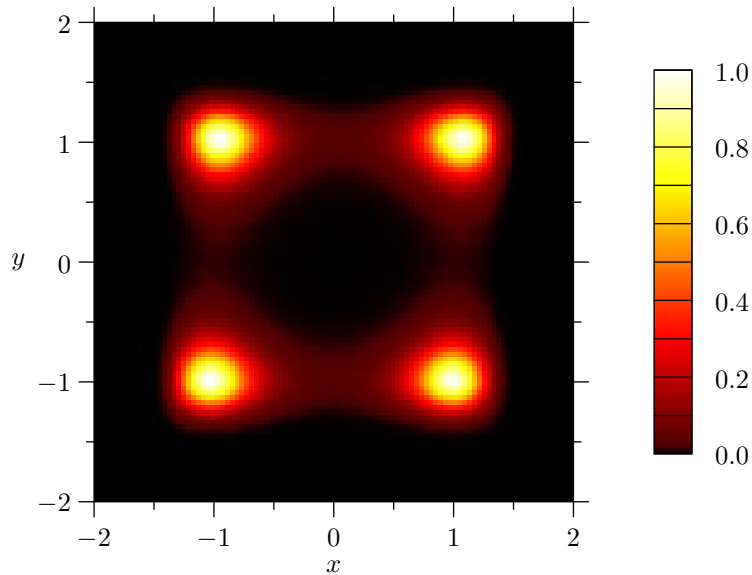


FIG. 4.2. The invariant density of the system (4.4)–(4.5) with  $\epsilon = 0.01$ ,  $a = 0.02$ , and  $\sigma^2 = 0.113$ . Computed using Ulam’s method with a flow time of  $\tau = 0.04$ . (See Section 6 for numerical details.)

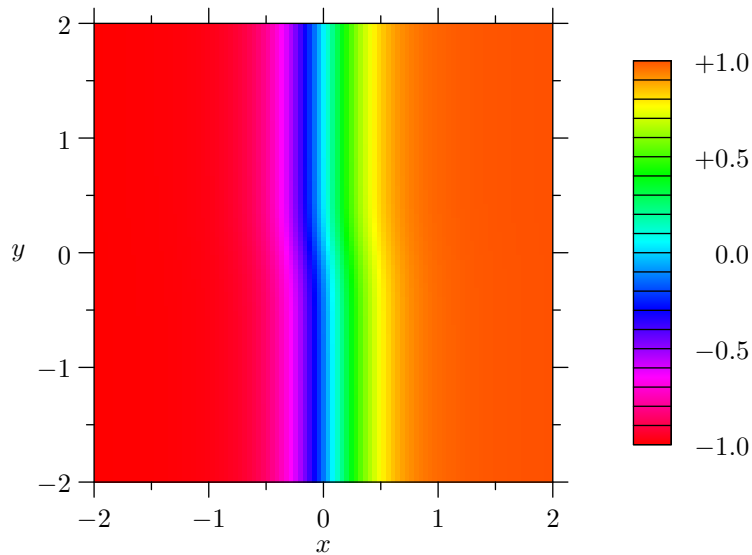


FIG. 4.3. The second eigenfunction of the Koopman operator for the system (4.4)–(4.5) with  $\epsilon = 0.01$ ,  $a = 0.02$ , and  $\sigma^2 = 0.113$ . Computed using Ulam’s method with a flow time of  $\tau = 0.04$ . (See Section 6 for numerical details.)

(over  $10^3$ ), and all within the same order of magnitude, which gives strong evidence the system has slow-fast behaviour with a time scale separation of between  $10^3$  and  $10^4$ . Compare this to the scaling term  $\epsilon^{-2} = 10^4$  in equation (4.5) and with the observed switching times for  $x$  and  $y$  in Figure 4.1.

As a further test that the fiber dynamics is a valid approximation of the fast

TABLE 4.1

Leading eigenvalues  $\lambda_i$  of the Koopman operator for the full two-dimension dynamics of the system (4.4)–(4.5) with  $\epsilon = 0.01$ ,  $a = 0.02$ , and  $\sigma^2 = 0.113$  with flow time  $\tau = 0.04$ . Also computed are the flow-independent values  $\chi_i = -\frac{1}{\tau} \log |\lambda_i|$  corresponding to the infinitesimal generator of the Koopman operator. Next, are the leading eigenvalues of the Koopman operator of the fiber dynamics computed with flow time  $\hat{\tau} = 4 \times 10^{-5}$  and the corresponding  $\hat{\chi}_i = -\frac{1}{\hat{\tau}} \log |\hat{\lambda}_i|$ . Here, the fiber  $\phi^{-1}(\{v\})$  is for  $v = 0.8$  where  $\phi$  is the eigenfunction plotted in Figure 4.3. The final column shows the ratio  $\hat{\chi}_i/\chi_i$ .

Full dynamics		Fiber dynamics		Ratio
$\lambda_i$	$\chi_i$	$\hat{\lambda}_i$	$\hat{\chi}_i$	$\hat{\chi}_i/\chi_i$
1.0000	0	1.0000	0	—
0.9995	$1.25 \times 10^{-2}$	0.9979	$5.26 \times 10^1$	$4.20 \times 10^3$
0.9665	$8.52 \times 10^{-1}$	0.7212	$8.17 \times 10^3$	$9.59 \times 10^3$
0.9429	1.47	0.5838	$1.35 \times 10^4$	$9.15 \times 10^3$
0.9153	2.21	0.4694	$1.89 \times 10^4$	$8.55 \times 10^3$
0.8801	3.19	0.3463	$2.65 \times 10^4$	$8.30 \times 10^3$
0.8397	4.37	0.2424	$3.54 \times 10^4$	$8.11 \times 10^3$
0.7954	5.72	0.1619	$4.55 \times 10^4$	$7.95 \times 10^3$
0.7477	7.27	0.1055	$5.62 \times 10^4$	$7.74 \times 10^3$
0.6969	9.02	0.0646	$6.85 \times 10^4$	$7.59 \times 10^3$

dynamics, we populated the fiber with  $10^4$  points  $\{z_i\}$  distributed in proportion to the computed invariant density of the system, and then computed  $\|T(z_i) - z_i\|$  and  $\|\hat{T}(z_i) - T(z_i)\|$  for each point. For this example, the average value of  $\|T(z_i) - z_i\|$  was  $3.69 \times 10^{-2}$  and the average value of  $\|\hat{T}(z_i) - T(z_i)\|$  was  $4.69 \times 10^{-4}$ . Further, the maximum value of  $\|\hat{T}(z_i) - T(z_i)\|$  over all of the points  $z_i$  was  $1.26 \times 10^{-2}$ . This shows that the fiber dynamics  $\hat{T}$  closely approximates  $T$ .

**4.3.3. A “slow-slow” system.** We now show that the same procedure when applied to a system without multiscale behaviour gives noticeably different results. As with the last example, consider the system defined by (4.4)–(4.5), but now set  $\epsilon = 1$  and  $a = 5$ . The value  $\sigma^2 = 0.113$  is as before. Under these parameters,  $y$  stays near  $+1$  or  $-1$  for long periods of time and, because of the term  $\frac{a}{\epsilon}y$  in (4.4), the  $x$  variable is now highly correlated with  $y$ . This system does not exhibit multiscale behaviour.

As with the last example, we computed eigenfunctions and then populated a fiber  $\phi^{-1}(\{v\})$  with  $10^4$  points  $\{z_i\}$  distributed in proportion to the computed invariant density of the system, and then computed  $\|T(z_i) - z_i\|$  and  $\|\hat{T}(z_i) - T(z_i)\|$  for each point. In this case, the average value of  $\|T(z_i) - z_i\|$  was  $5.36 \times 10^{-3}$  and the average value of  $\|\hat{T}(z_i) - T(z_i)\|$  was  $5.34 \times 10^{-3}$ . These values are nearly equal, showing that the full dynamics does not stay close to the fiber on short time scales, and that  $\hat{T} = \pi \circ T$  is not a valid approximation of the dynamics.

Applying Algorithm 1 produces eigenvalues as shown in Table 4.2. One should not read too much into the table, as the fiber dynamics do not meaningfully correspond to any form of “fast” dynamics, but notice that the ratios  $\hat{\chi}_i/\chi_i$  are not large in general and that the first ratio  $\hat{\chi}_2/\chi_2 \approx 197.37$  is of significantly different order than the others.

**4.3.4. A distorted example.** A major advantage of our approach to identifying and analyzing slow-fast systems is that the techniques are independent of the choice of coordinates and therefore the slow and fast directions do not need to align with

TABLE 4.2

Leading eigenvalues  $\lambda_i$  of the Koopman operator for the full two-dimension dynamics of the “slow-slow” system (4.4)–(4.5) with  $\epsilon = 1$ ,  $a = 5$ , and  $\sigma^2 = 0.113$  with flow time  $\tau = 0.04$ . Also computed are the flow-independent values  $\chi_i = -\frac{1}{\tau} \log |\lambda_i|$  corresponding to the infinitesimal generator of the Koopman operator. Next, are the leading eigenvalues of the Koopman operator of the fiber dynamics also computed with flow time  $\hat{\tau} = 0.04$  and the corresponding  $\hat{\chi}_i = -\frac{1}{\hat{\tau}} \log |\hat{\lambda}_i|$ . The final column shows the ratio  $\hat{\chi}_i/\chi_i$ .

Full dynamics		Fiber dynamics		Ratio
$\lambda_i$	$\chi_i$	$\hat{\lambda}_i$	$\hat{\chi}_i$	$\hat{\chi}_i/\chi_i$
1.0000	0	1.0000	0	—
0.9997	$7.50 \times 10^{-3}$	0.9425	1.48	197.37
0.9674	$8.29 \times 10^{-1}$	0.8105	5.25	6.34
0.9479	1.34	0.7019	8.85	6.62
0.9470	1.36	0.5365	15.6	11.43
0.9254	1.94	$0.5090 + 0.0237i$	16.9	8.70
$0.8983 + 0.0411i$	2.66	$0.5090 - 0.0237i$	16.9	6.39
$0.8983 - 0.0411i$	2.66	$0.4903 + 0.0814i$	17.5	6.58
0.8961	2.74	$0.4903 - 0.0814i$	17.5	6.37
0.8647	3.63	$0.4676 + 0.1403i$	17.9	4.93

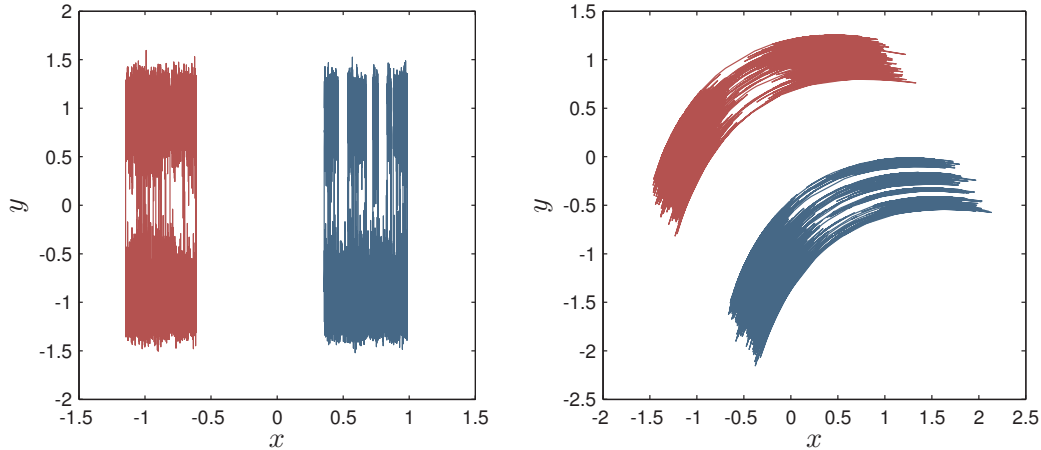


FIG. 4.4. Two finite orbits of the system (4.4)–(4.5) with  $\epsilon = 0.01$ ,  $a = 0.02$ , and  $\sigma^2 = 0.113$  before and after applying the distortion  $g$  described in Section 4.3.4. Each orbit represents flowing for one unit of time, and the two orbits were chosen to demonstrate the behaviour of the system near the two slow metastable states.

coordinate axes in order for the analysis to work. To demonstrate this, we apply a transformation to system (4.4)–(4.5). Recall that in Section 4.3.2, we treated the SDE (4.4)–(4.5) as a black box. Given a point  $z \in \mathbb{R}^2$ , we have an opaque method for computing the point  $T(z)$  which is the evolution after a time-step  $\Delta t = 2 \times 10^{-6}$ .

In place of  $z \mapsto T(z)$  consider instead,  $z \mapsto g \circ T \circ g^{-1}(z)$  where  $g$  is a diffeomorphism of the domain  $\mathbb{R}^2$ . This changes the coordinates without actually changing the dynamics. We take  $g$  to be the composition  $h \circ R$ , where  $h(x, y) = (x + 0.3y^2, y)$  and  $R$  is an irrational rotation of the plane (specifically, a clockwise rotation by one radian). Figure 4.4 shows this distortion applied to two orbits of the system.

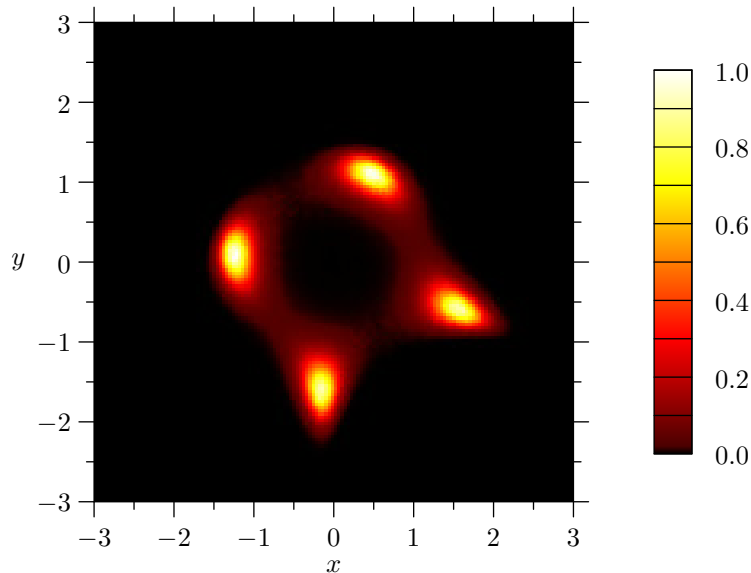


FIG. 4.5. The invariant density of the system (4.4)–(4.5) with  $\epsilon = 0.01$ ,  $a = 0.02$ , and  $\sigma^2 = 0.113$  after distortion. The distortion comes from conjugating the dynamics by the diffeomorphism  $g$  defined in Section 4.3.4. The density is computed by Ulam’s method applied to the distorted system using a flow time of  $\tau = 0.04$ .

TABLE 4.3

Leading eigenvalues for the Koopman operator of the full system and fiber dynamics as described in Algorithm 1. These eigenvalues are computed using Ulam’s method with axis-aligned boxes for the original system (4.4)–(4.5) with  $\epsilon = 0.01$ ,  $a = 0.02$ , and  $\sigma^2 = 0.113$  and for the same system conjugated by the diffeomorphism  $g : \mathbb{R}^2 \rightarrow \mathbb{R}^2$  defined in Section 4.3.4.

Full Dynamics ( $\tau = 0.04$ )		Fiber Dynamics ( $\hat{\tau} = 4 \times 10^{-5}$ )	
original	distorted	original	distorted
1.0000	1.0000	1.0000	1.0000
0.9995	0.9994	0.9979	0.9980
0.9665	0.9663	0.7212	0.7230
0.9429	0.9423	0.5838	0.5838
0.9153	0.9148	0.4694	0.4675
0.8801	0.8787	0.3463	0.3461
0.8397	0.8385	0.2424	0.2423
0.7954	0.7939	0.1619	0.1615
0.7477	0.7454	0.1055	0.1027
0.6969	0.6944	0.0646	0.0634

It is not immediately clear in the distorted picture where exactly the slow and fast directions lie. Still, we can apply Ulam’s method to calculate the eigenfunctions of the transfer and Koopman operators, as illustrated in Figures 4.5 and 4.6. The leading eigenvalues should, of course, be the same as in the original system, and computation confirms that, as shown in Table 4.3.

Using the second eigenfunction of the Koopman operator, we compute fiber dy-

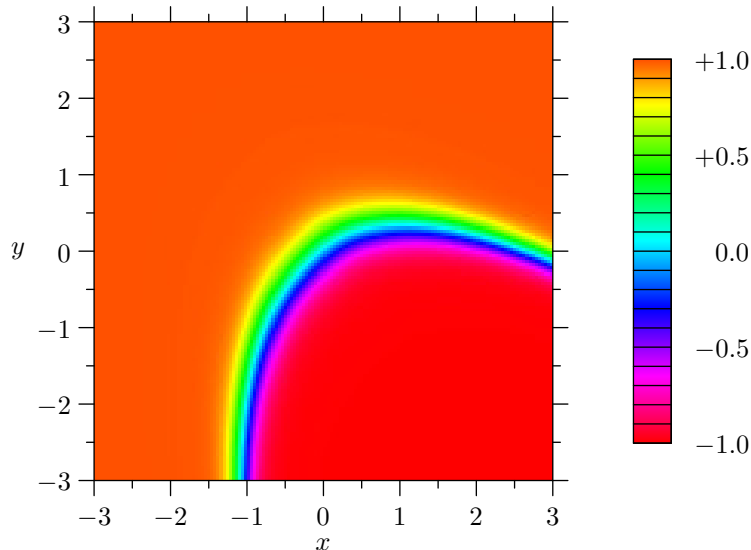


FIG. 4.6. The second eigenfunction of the Koopman operator for the system (4.4)–(4.5) with  $\epsilon = 0.01$ ,  $a = 0.02$ , and  $\sigma^2 = 0.113$  after distortion. The distortion comes from conjugating the dynamics by the diffeomorphism  $g$  defined in Section 4.3.4. The eigenfunction is computed by Ulam’s method applied to the distorted system using a flow time of  $\tau = 0.04$ .

namics as before. Eigenvalues associated to the fiber dynamics are computed and are nearly identical to the eigenvalues computed for the undistorted system. This shows that this technique of comparing eigenvalues to detect multiscale systems is independent of the choice of coordinates.

As before, we tested the validity of the fiber dynamics by populating a fiber with  $10^4$  points  $\{z_i\}$  distributed in proportion to the computed invariant density of the system, and then computed  $\|T(z_i) - z_i\|$  and  $\|\hat{T}(z_i) - T(z_i)\|$  for each point. For the distorted system, the average value of  $\|T(z_i) - z_i\|$  was  $4.37 \times 10^{-2}$  and the average value of  $\|\hat{T}(z_i) - T(z_i)\|$  was  $2.99 \times 10^{-4}$ . Further, the maximum value of  $\|\hat{T}(z_i) - T(z_i)\|$  over all of the points  $z_i$  was  $1.26 \times 10^{-2}$ . This shows that, as in the undistorted case, the fiber dynamics  $\hat{T}$  closely approximates  $T$ .

**5. Reduced dynamics.** The fiber dynamics approach studied in the previous sections gives a good way to isolate the fast dynamics of the system. We also want to efficiently emulate the slow dynamics of the system using a large time step. To do this, we assume the slow dynamics of the system is well approximated by a drift-diffusion process. The details and justification of this approach will be given later in the section, but we first list the proposed algorithm here:

**Algorithm 2**

1. Numerically compute the invariant density  $\rho$  of the dynamical system  $T$ .
2. Numerically compute an approximate eigenfunction  $\phi$  of the Koopman operator associated to an eigenvalue close to one.
3. Reparameterize  $\phi$  to yield a function  $\theta$  which varies evenly throughout the domain.
4. Compute fibers for  $\theta$ .
5. For each computed fiber  $\theta^{-1}(\{v\})$ :
  - (a) Populate  $\theta^{-1}(\{v\})$  by an ensemble of points  $\{z_i\}_{i=1}^q$  sampled in propor-

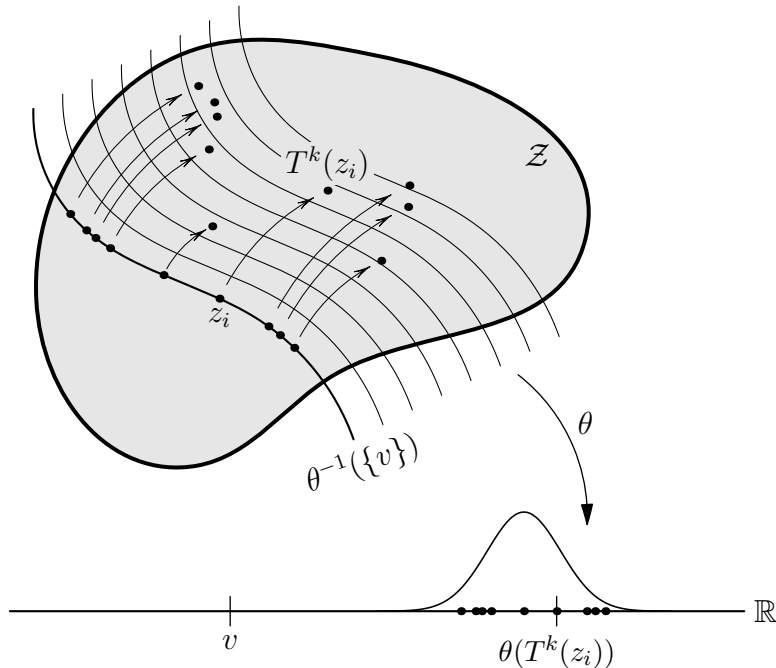


FIG. 5.1. An illustration depicting Algorithm 2.

tion to the invariant density  $\rho^1$ .

- (b) Iterate each point  $z_i$  forward by  $T^k$  and project by  $\theta$ .
- (c) Compute  $\alpha_k(v)$  and  $\beta_k(v)$  as the mean and variance of the ensemble  $\{\vartheta_i\}_{i=1}^q = \{\theta(T^k(z_i)) - v\}_{i=1}^q$ . That is,

$$\alpha_k(v) = \frac{1}{q} \sum_i \vartheta_i \quad \text{and} \quad \beta_k(v) = \frac{1}{q} \sum_i (\vartheta_i - \alpha_k(v))^2.$$

- 6. Extend  $\alpha_k$  and  $\beta_k$  by linear interpolation to functions on  $\mathbb{R}$ .
- 7. Use  $\alpha = \alpha_k/k\Delta t$  and  $\beta = \beta_k/k\Delta t$  to define a drift-diffusion process

$$dX_t = \alpha(X_t)dt + \sqrt{\beta(X_t)}dW_t$$

representing the reduced slow dynamics.

A visual depiction of this algorithm is given in Figure 5.1.

Let us first comment on Step 3 of the algorithm and how we define the projection  $\theta$ . Since we are assuming fast dynamics occurs along the level sets of an eigenfunction  $\phi$  of the Koopman operator, this function  $\phi$  presents a natural choice for projection to a one-dimensional space for the slow dynamics, as discussed in Section 4.1. However, this is not an ideal candidate for numerical calculation in systems with meta-stable slow states: Suppose the dynamical system has two metastable states in the slow

<sup>1</sup>Alternatively one could use the fast fiber dynamics defined in Section 4.1 to compute the invariant density on each fast fiber  $F$ . However, this is computationally much more involved and we therefore use the invariant density of the full dynamics.



direction, as in the equations (4.4)–(4.5). The eigenfunction  $\phi$ , after scaling, will be close to  $+1$  near one of the metastable states, close to  $-1$  near the other, and change sharply in the area where it transitions from one state to the other. Such a sharp change is visible in Figure 4.3. In fact, such regions where an eigenfunction is nearly constant can be used to detect the existence of such metastable states and of “almost invariant sets” [15, 25]. For our purpose, however, those regions make it hard numerically to use  $\phi$  as a projection.

To overcome this problem, we replace  $\phi$  by a function which has similar level sets, but which varies evenly throughout the phase space.

Suppose  $\phi$  is represented numerically by its values on a finite grid of points  $\{z_i\}_{i=1}^M$  in the phase space  $\mathcal{Z}$ . Then, we define the function  $\theta : \{z_i\}_{i=1}^M \rightarrow \{1, \dots, M\}$  as a bijection of finite sets and such that  $\phi(z_i) < \phi(z_j)$  implies  $\theta(z_i) < \theta(z_j)$ . That is, from  $\phi$  we have extracted only its ordering of points on the grid. To get a suitable continuous function, extend  $\theta$  to the rest of the phase space by linear interpolation in each coordinate. Let  $B \subset \mathbb{R}^d$  be the box on which the grid of points lies. Then, one way of thinking about this step, is that we are replacing  $\phi$  by some reparameterization  $\theta = h \circ \phi$  with  $h : \mathbb{R} \rightarrow \mathbb{R}$  a homeomorphism, so that for an interval  $[a, b] \subset \mathbb{R}$  the volume of  $\theta^{-1}([a, b]) \cap B$  is roughly proportional to the length of  $[a, b]$ .

For example, the eigenfunction plotted in Figure 4.3 was computed using a 200 by 200 grid  $G$  of points  $z_i = (x_i, y_i) \in \mathbb{R}^2$ . The relative ordering of the values  $\phi(x_i, y_i)$  on this grid  $G$  defines a bijection  $\theta : G \rightarrow \{1, \dots, 40\,000\}$  which extends to the convex hull of  $G$  by bilinear interpolation. Such a construction would yield a  $\theta$  ranging between 1 and 40 000. As a further step, we rescale  $\theta$  so that it ranges between  $-4$  and  $+4$ . This makes it easier to allow for an easier comparison between  $\theta(T^k(z_i))$  and the original slow  $x$ -variable in (4.4)–(4.5).

Algorithm 2 relies on the reduced system being a stochastic differential equation. Diffusion limits of stochastic multiscale systems such as (4.4)–(4.5) have been rigorously established in the framework of homogenization (see, for example, [31, 57]) in the limit  $\epsilon \rightarrow 0$ . Diffusion limits for deterministic dynamical systems have also been established [47, 33] and have been extended to the discrete time case as well [33]. Assuming, then, that the slow dynamics is well modelled by a one-dimensional drift-diffusion system, our algorithm describes how to estimate the drift term  $\alpha(X)$  and the diffusion term  $\beta(X)$  in

$$(5.1) \quad dX_t = \alpha(X_t)dt + \sqrt{\beta(X_t)}dW_t$$

so that an orbit of this process closely resembles the projection under  $\theta$  of an orbit of the full system.

We estimate  $\alpha$  and  $\beta$  at  $v \in \mathbb{R}$  by ensemble averages over an ensemble

$$\{X_{t_k, i}\}_{i=1}^q$$

of size  $q$ . The ensemble is generated as follows (cf. Figure 5.1): Populate the fiber  $F$  by a number of points  $z_i$ , evolve each point forward by  $k$  time-steps of the computation to a point to  $T^k(z_i)$  at time  $t_k$ , and then project onto the slow subspace using the projection  $\theta$  to yield  $\theta(T^k(z_i))$ . The initial population of points  $\{z_i\}_{i=1}^q$  on  $F$  should be chosen in proportion to the invariant density function computed for the full dynamics (or the dynamics on the fast fibers). We remark that this procedure bears resemblance with the equation-free approach proposed in [30, 36, 35].

The drift and diffusion coefficients  $\alpha(v)$  and  $\beta(v)$  are then approximated for small

times  $t_k$  by  $\alpha_k(v)/t_k$  and  $\beta_k(v)/t_k$  where  $\alpha_k(t_k)$  and  $\beta_k(t_k)$  are the mean and variance of  $\{X_{t_k,i} - v\}_{i=1}^q$  [28].

Note that in general the variance of  $\{X_{t_k,i} - v\}_{i=1}^q$  would depend on the drift term as well as the diffusion term in 5.1; however for small times  $t_k$  we can assume that the slow variables  $X_t$  is constant and the diffusion term will dominate so that  $\beta(X)$  can be determined as the ensemble average of the variance of  $\{X_{t_k,i} - v\}_{i=1}^q$ .

Let us now comment on the choice of the flow time  $t_k$  (or the number of iterations,  $k$ ). The definition of the drift and diffusion coefficients requires  $t_k \rightarrow 0$  [28]. However, to capture time scales which go beyond the fast time scale, i.e., times which are sufficiently large to allow for equilibration on each fast fiber,  $t_k$  needs to be sufficiently large. In the context of the particular scaling of the multiscale system (4.4)–(4.5) we require  $t_k \sim \mathcal{O}(1/\epsilon)$ , which is long enough that the fast variables behave according to the invariant density on each fiber and small enough to allow for (nearly) constant slow variables. For such times the diffusion term in the reduced dynamics is expected to be dominant; hence we chose  $t_k$  such that the set of values  $\theta(T^k(z_i))$  has a distribution close to normal. To test for normality we use the Lilliefors test for normality [42]. In many cases, the Lilliefors test and the Kolmogorov–Smirnov test on which it is based are used to test the hypothesis that a given finite set of points was sampled from a normal distribution. In our situation, the projection of the dynamics only approximates a normal distribution and it is not helpful to calculate the probability that such a population came from a true normal distribution. Instead, we consider the test statistic used in the Lilliefors test, which is a positive number computed from the sample, and use that this test statistic is closer to zero when the sample is closer to normal. In Figure 5.2 we show how  $t_k$  can be chosen as the time where the Lilliefors test statistics has a minimum.

In the framework for slow-fast systems introduced in Section 2, the drift-diffusion process (5.1) now plays the role of the reduced dynamical system  $S$  on the reduced space  $\mathcal{X} = \mathbb{R}$  and the map  $\mathcal{P} : \mathcal{Z} \rightarrow \mathcal{X}$  is given by  $\theta$ . By the assumption  $\mathcal{P} \circ T^N \approx S \circ \mathcal{P}$  for large  $N$ , if  $k$  is sufficiently large, then for a point  $z \in \theta^{-1}(\{v\})$ , the value  $\theta(T^k(z))$  gives an approximation of the result of evolving (5.1) forward by a time  $t$  proportional to  $k$  from the starting value  $X_0 = v$ . Thus, the computation  $v \rightsquigarrow z_i \rightsquigarrow \theta(T^k(z_i))$  in Step 5 of Algorithm 2 provides the ensemble  $\{X_{t_k,i}\}$  described above.

## 5.1. Examples.

**5.1.1. The skew-product example.** We now apply Algorithm 2 to the example system (4.4)–(4.5) from Section 4.3.2. For this system, Figure 5.2 plots how the test statistic varies in the number of iterates  $k$  for a sample of points on a fast fiber  $F = \theta^{-1}(\{v\})$ . For  $k = 0$ , every point  $z_i$  projects to the same value in  $\mathbb{R}$ . As  $k$  increases, the distribution becomes more normal as the values  $\theta(T^k(z_i))$  spread out. However, as  $k$  becomes very large, the distribution of the points starts to approach the invariant density of the full system, and this density, when projected by  $\theta$ , will in general not be normal. From the graph, a value of  $k = 10^5$  iterates gives a distribution which is close to normal. That the test statistic is low here ( $\sim 0.02$ ) gives empirical support to the assumption that the slow dynamics can be well approximated by a drift-diffusion process.

For simplicity, we assume that the same value  $k$  can be used for all fibers, as is the case for this example. For Step 5 of Algorithm 2, we used 500 fibers with the

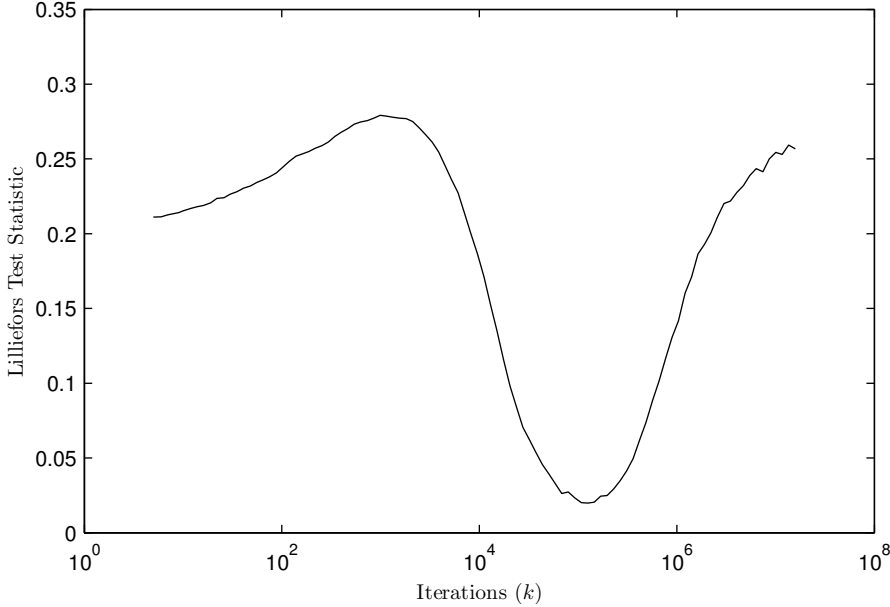


FIG. 5.2. The Lilliefors test statistic for the ensembles  $\{\theta(T^k(z_i))\}$  described in Algorithm 2. A lower test statistic indicates the distribution is closer to normal. One iterate corresponds to a time step  $\Delta t = 2 \times 10^{-6}$  of the system (4.4)–(4.5) with  $\epsilon = 0.01$ ,  $a = 0.02$ , and  $\sigma^2 = 0.113$ .

value  $v$  varying between  $-4$  and  $4$ . Each fiber was populated with  $q = 10^4$  points. The resulting functions  $\alpha_k$  and  $\beta_k$  are plotted in Figure 5.3.

If  $k$  iterations corresponds to a change in time  $k\Delta t$ , then  $\alpha$  and  $\beta$  in (5.1) can be approximated by  $\frac{\alpha_k}{k\Delta t}$  and  $\frac{\beta_k}{k\Delta t}$ . Note that while the diffusion function  $\beta$  would be constant for the homogenization limit of (4.4)–(4.5) as  $\epsilon \rightarrow 0$ , the computed function  $\beta_k$  in Figure 5.3 is non-constant because it is computed using a non-zero time-step  $k\Delta t$  which causes enhanced diffusion near the saddle point which separates the two metastable states near  $x = \pm 1$ .

The drift-diffusion process (5.1) can now be used to simulate the slow dynamics using a time step which would be too large to simulate the full dynamics. Here, we use a time step of  $dt = 0.02$  and calculate the orbit by

$$(5.2) \quad v_{n+1} = v_n + \alpha(v_n) dt + \sqrt{\beta(v_n) dt} r_n$$

where the  $r_n$  are independent pseudo-random values drawn from the standard normal distribution. Such a simulated orbit is plotted in Figure 5.4. This simulated orbit closely resembles the slow  $x$  variable of the original system (shown in Figure 4.1).

**5.1.2. A distorted example.** Finally, we use Algorithm 2 to simulate a slow orbit of the distorted system of Section 4.3.4. The computed functions for the drift  $\alpha_k$  and diffusion  $\beta_k$  are plotted in Figure 5.5 and a simulated orbit of the reduced system is plotted in Figure 5.6. As in Section 4.3.4, our algorithm is insensitive to non-trivial coordinate transformations and accurately distills the slow variables and their dynamics.

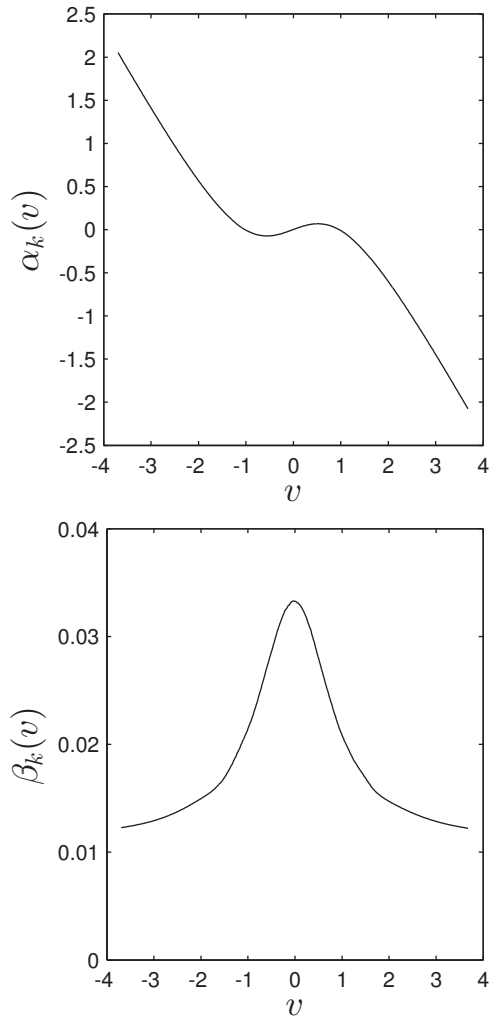


FIG. 5.3. The drift  $\alpha_k$  and diffusion  $\beta_k$  computed in Algorithm 2 for the system (4.4)–(4.5) with  $\epsilon = 0.01$ ,  $a = 0.02$ , and  $\sigma^2 = 0.113$ .

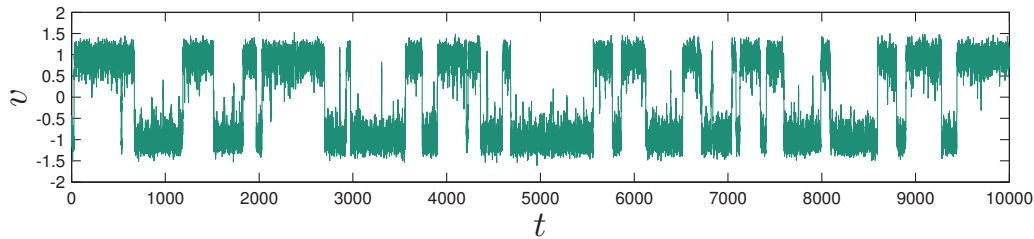


FIG. 5.4. Simulation of an orbit of the reduced one-dimensional dynamics given by Algorithm 2 for the system (4.4)–(4.5) with  $\epsilon = 0.01$ ,  $a = 0.02$ , and  $\sigma^2 = 0.113$ . The orbit was calculated using (5.2) with  $dt = 0.02$ .

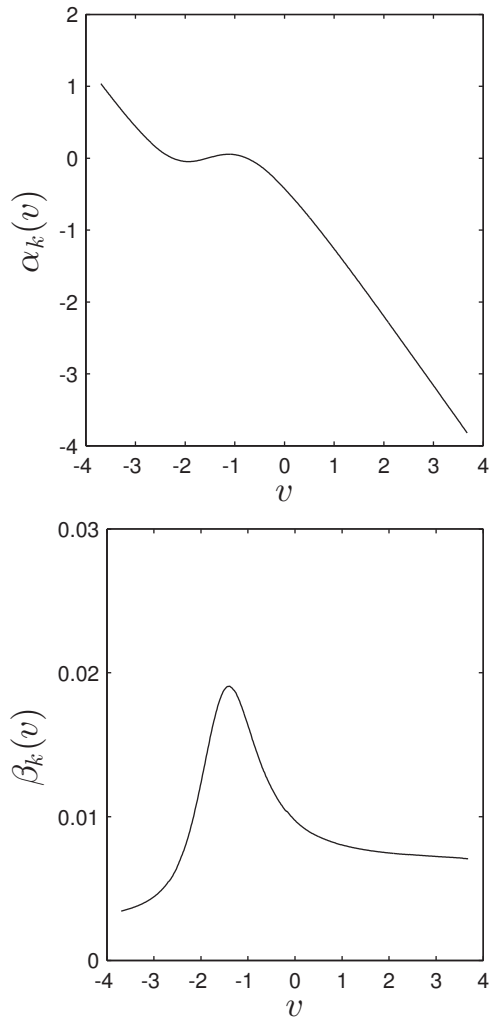


FIG. 5.5. The drift  $\alpha_k$  and diffusion  $\beta_k$  computed in Algorithm 2 for system (4.4)–(4.5) with  $\epsilon = 0.01$ ,  $a = 0.02$ , and  $\sigma^2 = 0.113$  after distortion. The distortion comes from conjugating the dynamics by the diffeomorphism  $g$  defined in Section 4.3.4.

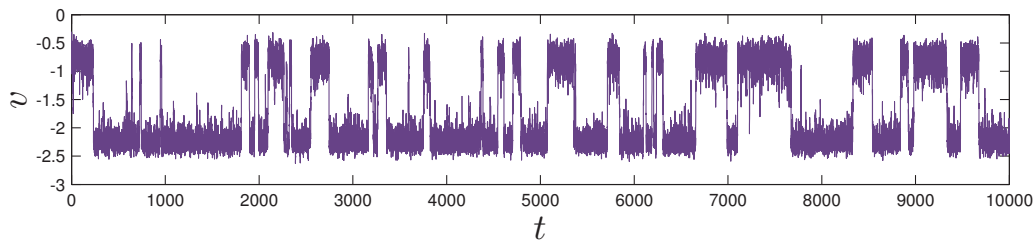


FIG. 5.6. Simulation of an orbit of the reduced one-dimensional dynamics given by Algorithm 2 for system (4.4)–(4.5) with  $\epsilon = 0.01$ ,  $a = 0.02$ , and  $\sigma^2 = 0.113$  after distortion. The distortion comes from conjugating the dynamics by the diffeomorphism  $g$  defined in Section 4.3.4. The orbit was calculated using (5.2) with  $dt = 0.02$ .

**5.2. Statistics.** From a visual comparison of Figures 4.1, 5.4, and 5.6, it is not entirely clear if the reduced dynamics of Algorithm 2 is accurately capturing behaviour of the slow variable  $x$  in (4.4)–(4.5). To be more certain, we compute statistics related to these time series.

As argued in Section 4, the eigenvalue  $\phi$  of the Koopman operator is approximately equal to  $\psi \circ \mathcal{P}$  where  $\psi$  is an eigenfunction for the reduced dynamics and  $\mathcal{P} : \mathcal{Z} \rightarrow \mathcal{X}$  is the mapping down to the reduced space. Algorithm 2 replaces  $\phi$  with a function  $\theta$  which has similar level sets. Therefore,  $\theta$  should be of the form  $\theta = h \circ \mathcal{P}$  for some unknown  $h$ . Because of this, when comparing time series of the full dynamics with time series for the reduced dynamics, one should only use statistics which are unchanged when  $\mathcal{P}$  is replaced with  $h \circ \mathcal{P}$  where  $h$  is a homeomorphism of the real line.

In our case, an obvious choice for such a statistic is the average switching time between the two metastable states. From a time series  $\{v_i\}_{i=1}^M$ , such as those plotted in Figures 4.1, 5.4, and 5.6, compute percentiles  $v^-$  and  $v^+$  such that 40% of the points in  $\{v_i\}$  are below  $v^-$  and 60% are below  $v^+$ . Then, declare each point  $v_i$  to be in either the “high” state or the “low” state by the following heuristic:

- if  $v_i \geq v^+$ , then  $v_i$  is in the high state,
- if  $v_i \leq v^-$ , then  $v_i$  is in the low state,
- otherwise,  $v_i$  is in the same state as  $v_{i-1}$ .

This gives us a way to measure the switching times which is unaffected by applying a homeomorphism  $h : \mathbb{R} \rightarrow \mathbb{R}$  to the time series.

For the full dynamics (4.4)–(4.5) with  $\epsilon = 0.01$ ,  $a = 0.02$ , and  $\sigma^2 = 0.113$ , we computed a time series  $\{x_i\}_{i=1}^M$  of the  $x$ -variable with  $M = 2 \times 10^6$  and where each step  $x_i$  to  $x_{i+1}$  represents a change of time of  $\tau = 0.2$ . This involved  $2 \times 10^{11}$  individual steps of the Euler-Maruyama method, using  $\Delta t = 2 \times 10^6$ . For the reduced dynamics, a similar time series  $\{v_i\}_{i=1}^M$  with the same  $M = 2 \times 10^6$  and  $\tau = 0.2$  were obtained. Each step  $v_i$  to  $v_{i+1}$  was computed by ten applications of (5.2), each with a time step of  $dt = 0.02$ .

For the full time series, there were 2222 switches between the metastable states, with a mean switching time of  $\tau_0 = 180.0$ . For the reduced dynamics of Section 5.1.1, there were 2280 switches with a mean time of  $\tau_0 = 175.5$ . In the distorted case in Section 5.1.2, there were 2178 switches with a mean time of  $\tau_0 = 183.7$ .

In each case, we expect the switching times  $\tau_i$  to obey a Poisson process, where the cumulative probability function is given by the formula

$$P_c(\tau_i) = 1 - \exp\left(-\frac{\tau_i}{\tau_0}\right)$$

where  $\tau_0$  is the mean switching time. To see if this the case, the computed switching times  $\tau_i$  are plotted against  $-\log(1 - P_c(\tau_i))$ , as shown in Figure 5.7. For each of the three time series, the resulting plot is linear, and a least squares fit gives a computed value for  $\tau_0 = 177.3$  for the full dynamics  $\{x_i\}$  of Section 4.3.2,  $\tau_0 = 178.8$  for the reduced dynamics of Section 5.1.1, and  $\tau_0 = 182.2$  for the reduced dynamics of the distorted system in Section 5.1.2.

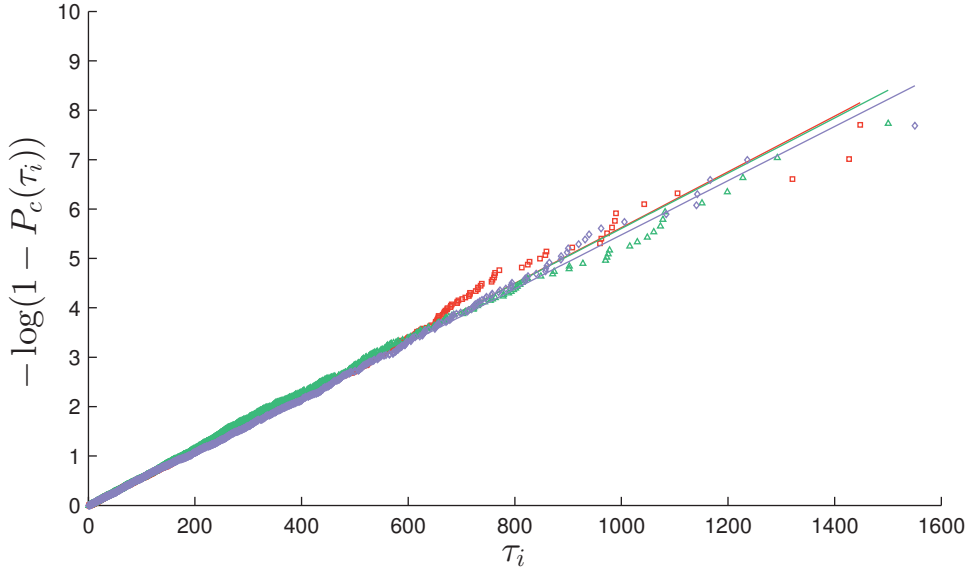


FIG. 5.7. Log plot of the normalized histogram of switching times  $\tau_i$ . This is computed for time series of the  $x$  variable of (4.4)–(4.5) as in Section 4.3.2 (red squares), for the reduced dynamics in Section 5.1.1 (green triangles) and for the reduced dynamics of the distorted system in Section 5.1.2 (blue diamonds).

**6. Computing the eigenfunctions.** The techniques in this paper use spectral properties of the transfer operator, and its adjoint, the Koopman operator. Therefore, we must approximate these operators numerically. There are a number of approaches that could be used, and specialized methods other than Ulam, may be significantly faster in certain settings, depending on the smoothness of the system. These include numerical methods based on the infinitesimal generator of Ulam’s method [24], finite-element methods [2], and Galerkin methods using Fourier or Chebyshev bases [8]. See also Chapter 5 of [39]. For simplicity, we employ the standard Ulam’s method [63, 41] for all of the examples in this paper. Eigenpairs and the level sets were computed using the `eigs` and `contour` routines of MATLAB [46].

Recall that for a deterministic dynamical system  $T : \mathcal{Z} \rightarrow \mathcal{Z}$ , the transfer (or Perron-Frobenius) operator  $\mathcal{L}$  on  $L^2(\mathcal{Z})$  is defined by

$$(6.1) \quad \int g \cdot \mathcal{L}f \, dm = \int (g \circ T) \cdot f \, dm$$

for all  $f, g$  in  $L^2(\mathcal{Z})$ . To solve numerically, Ulam’s method divides the domain  $\mathcal{Z}$  into a finite number of boxes  $B_1, \dots, B_n$  and reduces the problem to

$$(6.2) \quad \int \mathbb{1}_{B_i} \cdot \mathcal{L}\mathbb{1}_{B_j} \, dm = \int (\mathbb{1}_{B_i} \circ T) \cdot \mathbb{1}_{B_j} \, dm$$

for  $i, j = 1, \dots, n$  and where  $\mathbb{1}_{B_i}$  is the indicator function for the set  $B_i$ . The resulting operator, now defined on the finite dimensional space spanned by the functions  $\mathbb{1}_{B_i}$  is equivalent to an  $n \times n$  matrix defined by

$$P_{ij} = \frac{m(T^{-1}(B_i) \cap B_j)}{m(B_i)}.$$

To estimate  $P_{ij}$  numerically, populate each  $B_j$  with a large number  $N$  of randomly sampled test points  $z_{j,k}$  for  $k = 1, \dots, N$  and use

$$(6.3) \quad P_{ij} \approx \frac{1}{N} \#\{k : T(z_{j,k}) \in B_i\}.$$

In the case of a random dynamical system, the dynamics is defined by a map  $T : \mathcal{Z} \times \Omega \rightarrow \mathcal{Z}$  where  $\Omega$  is a probability space, sometimes called the “noise space” of the system. Each  $\omega \in \Omega$  defines a function  $T_\omega = T(\cdot, \omega)$  and one can define a transfer operator  $\mathcal{L}_\omega$  for each  $T_\omega$ . We then consider the annealed (or integrated) operator  $\mathcal{L} : L^2(\mathcal{Z}) \rightarrow L^2(\mathcal{Z})$  defined by

$$\mathcal{L}(f) = \int_{\Omega} \mathcal{L}_\omega(f) d\omega.$$

Similarly, the annealed Koopman operator is

$$(\mathcal{K}f)(z) = \int_{\Omega} f(T(z, \omega)) d\omega$$

which for a point  $z$ , gives the expected value of  $f(T(z))$ . For a random dynamical system, Ulam’s method produces a matrix which can be approximated numerically by the slightly modified version of (6.3) with

$$(6.4) \quad P_{ij} \approx \frac{1}{N} \#\{k : T_{\omega_{j,k}}(z_{j,k}) \in B_i\},$$

where for each  $z_{j,k} \in B_j$ , the noise parameter  $\omega_{j,k} \in \Omega$  is chosen randomly and independently.

The examples in this paper are defined by stochastic differential equations. In this case, the noise space  $\Omega$  is the space of continuous paths  $C^0(\mathbb{R}, \mathbb{R}^d)$  where the probability measure is given by the Wiener process representing Brownian motion. Once a path  $W \in \Omega = C^0(\mathbb{R}, \mathbb{R}^d)$  is chosen, an SDE of the form

$$dx_t = \mu(x)dt + \sigma dW_t$$

at starting value  $x(0) = x_0$  is solved by a path satisfying the integral

$$x(t) = x_0 + \int_0^t \mu(x(s)) ds + \sigma W(t)$$

at all times  $t > 0$ . For a specified flow time  $\tau > 0$ , this gives a deterministic map  $T_W(x_0) = x(\tau)$  for each  $W \in \Omega$  and so defines a random dynamical system in the form  $T : \mathcal{Z} \times \Omega \rightarrow \mathcal{Z}$ . For each point  $z_{j,k}$  in (6.4), the image  $T_{\omega_{j,k}}(z_{j,k})$  can be computed, for example, by the Euler-Maruyama method [38], and so the annealed operators for these types of systems can be approximated numerically.

For these continuous-time dynamical systems, one must choose some interval of time  $\tau > 0$  in order to apply Ulam’s method to the map  $T = \varphi_\tau$  given by the flow  $\{\varphi_t\}_{t \in \mathbb{R}}$ . Picking too small a flow time can lead to a dynamical system appearing to have more diffusion than is actually present, a problem closely related to so-called “numerical diffusion” which appears in finite-difference methods [24]. A common practice is to choose  $\tau$  large enough, so that for a significant number of sample points  $x_{i,k} \in B_i$ , the image  $T(x_{i,k}) = \varphi_\tau(x_{i,k})$  is no longer inside the box  $B_i$  [25]. In other words, so that  $P_{ii}$  is not too close to one.



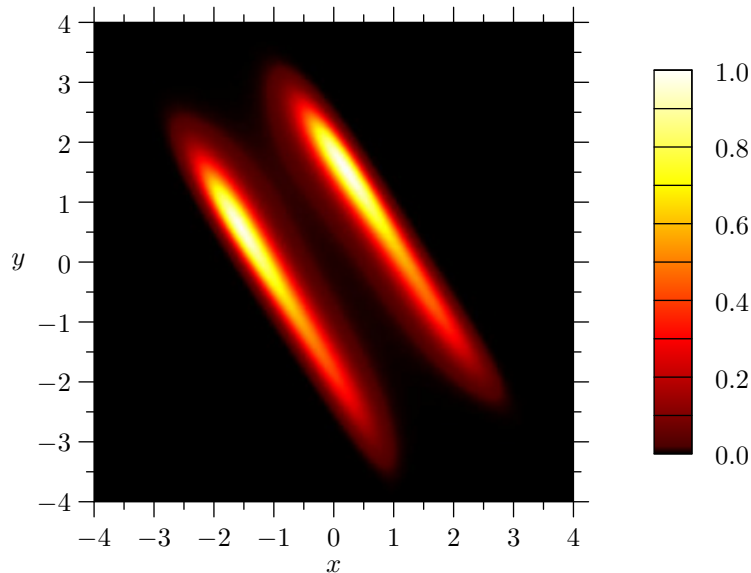


FIG. 6.1. An incorrect density calculated using Ulam's method with too short a flow time for system (4.4)–(4.5) with  $\epsilon = 0.01$ ,  $a = 0.02$ , and  $\sigma^2 = 0.113$  conjugated by the diffeomorphism  $g$  defined in Section 4.3.4. The flow time used to construct the Ulam matrix is  $\tau = 2 \times 10^{-5}$ . Compare this to the computed density in Figure 4.5.

This works well for many systems, but it is not a sufficient criterion for a system with multiscale behaviour. For these systems, choosing a flow time in such manner only guarantees that Ulam's method captures the fastest dynamics, and there may be significant numerical diffusion present in the direction of the slow dynamics, meaning that the computed invariant density and other eigenfunctions may have significant errors.

The effect is more pronounced when the slow and fast directions do not align with the grid of boxes. Here, Ulam's method cannot faithfully capture motion happening purely in the fast direction. In some sense, the Galerkin projection “smears” the point  $T(x_{i,k})$  over the box  $B_j$  in which it resides and this smearing happens in both slow and fast directions. As an example, we use Ulam's method for the system (4.4)–(4.5) after distortion as defined in Section 4.3.4 with an extremely short time-step of  $\tau = 2 \times 10^{-5}$ . In the resulting Ulam matrix, the maximum value  $P_{ii}$  on the diagonal is less than 0.11. However, the computed density, plotted in Figure 6.1, shows two thick spurious bands, which would be more consistent with a system with a large amount of diffusion in the slow direction (cf. the invariant density in Figure 4.5 computed with significantly larger flow time  $\tau = 0.04$ ).

One way to avoid this is to increase the flow time so that a typical point moves in the slow direction by an amount comparable to the size of the boxes  $B_i$ . However, we are assuming that we do not know in advance the directions of the slow and fast dynamics. To handle this, we compute unit eigenvectors using Ulam's method for a sequence of increasing flow times, and stop when the result stabilizes. For instance, in the axis-aligned example system (4.4)–(4.5) in Section 4.3.2, the invariant density  $\rho_\tau \in \text{span}\{\chi_1, \dots, \chi_n\} \subset L^1(\mathbb{R}^2)$  was computed for flow times  $\tau = 0.01, 0.02$ , and  $0.04$ . Using the  $L^1$  norm  $\|f\| = \int_{\mathbb{R}^2} |f(x)| dx$ , we compute  $\|\rho_{0.01} - \rho_{0.02}\| \cong 0.08$  and  $\|\rho_{0.02} - \rho_{0.04}\| \cong 0.03$ . More important than the density is the second

leading eigenfunction of the Koopman operator, i.e., the eigenfunction shown in Figure 4.3, since this function is used to define the fiber dynamics. The corresponding  $L^1$  differences for this computed eigenfunction are  $\|\phi_{0.01} - \phi_{0.02}\| \cong 0.04$  and  $\|\phi_{0.02} - \phi_{0.04}\| \cong 0.01$ . We view this difference as small enough that we can safely use  $\tau = 0.04$  in the computation of the eigenfunctions.

Because we are using the Euler-Maruyama method with a time-step of  $2 \times 10^{-6}$ , this value of  $\tau$  corresponds to  $2 \times 10^4$  iterations. However, this value of  $\tau$  is still much smaller than the average time an orbit takes to switch between the metastable states based at  $x = -1$  and  $x = +1$ . That switching happens on the order of hundreds of units of time (as shown in Figure 4.1).

As a further test, we also consider the computed eigenvalues. As argued in Section 3, the leading eigenvalues of the full dynamics correspond to decay rates associated to the slow dynamics. Therefore, if many of the computed eigenvalues are very close to one, it suggests that the flow time may be too short. For  $\tau = 0.04$  in the example system, the leading ten computed eigenvalues (as listed in Table 4.1) range from 1.000 to 0.6969 which is far enough from 1 to tell us that advection in the slow direction is being captured in the Ulam matrix.

In addition to choosing the flow time, one must also set the number of sample points  $N$  in (6.3) or (6.4). Because of the relatively long flow time, starting from one box  $P_{ij}$  the evolved points  $T(x_{i,k})$  may lie in a large number of boxes  $B_j$ , and  $N$  must be chosen large enough that each  $P_{ij}$  is computed to a reasonable accuracy. In all our examples, we use  $N = 10^4$  and a 200 by 200 grid on the region  $[-4, 4] \times [-4, 4] \subset \mathbb{R}^2$ . This is a much larger region than where orbits typically lie. However, we compute everything in this larger region so that when fiber dynamics are computed, the orbit will stay in the domain with very high probability.

Once a level set is computed, the same heuristics using  $L^1$ -distance of the computed eigenfunctions and the distance of the eigenvalues from 1 may be used to determine a reasonable number of iterations to apply for the fiber dynamics. These showed that 20 iterations for a total flow time of  $20 \times 2 \times 10^{-6} = 4 \times 10^{-5}$  was sufficient for the fiber dynamics of the example system (4.4)–(4.5) in Section 4.3.2.

An eigenfunction  $\phi$  computed using Ulam’s method will be given as a linear combination of the indicator functions  $\mathbb{1}_{B_i}$ . As such functions are piecewise-constant, the gradient  $\nabla\phi$  will therefore be zero anywhere it is defined. This gradient is not useful in defining a gradient flow  $\pi$  as used in Algorithm 1. Instead, when computing  $\nabla\phi$  for use in the algorithm we replace  $\phi$  by the bilinear interpolation of values it takes on the centers of each box  $B_i$ . Further, as solving for the gradient flow is computationally expensive, we employ the following shortcut. To compute the map  $\pi : U \rightarrow \phi^{-1}(\{v\})$  at a point  $z \in U$  evaluate the gradient at  $z$ , then take  $\pi(z)$  to be the intersection of the fiber  $\phi^{-1}(\{v\})$  with the line given by  $z + \mathbb{R} \cdot \nabla\phi(z)$ . Since in computing the fiber dynamics the function  $\pi$  is only evaluated at points very close to the level set, the gradient is nearly constant on the short path from  $z$  to  $\pi(z)$ , and so the approximation is valid.

Alternatively, at least in principle, one could have used the eigenfunctions of the transfer operator  $\mathcal{L}$  instead of those of the Koopman operator  $\mathcal{K}$ . If  $\mu$  is an invariant density for the dynamical system  $T$ , then (6.1) with  $m = \mu$  defines a transfer operator  $\mathcal{L}_\mu$  and the invariance of the measure implies that a constant function  $f \equiv c \in \mathbb{R}$  satisfies  $\mathcal{L}_\mu(f) = f$ . Numerical experiments suggest that, similar to the Koopman

operator, leading eigenfunctions of  $\mathcal{L}_\mu$  are nearly constant in the fast direction of a multiscale system. The problem with this approach is that one must numerically approximate the density  $\mu$ , say by a density function,  $\rho$ , and use this to compute eigenfunctions of  $\mathcal{L}_\mu$ . Numerically, this is equivalent to calculating the pointwise quotient  $\phi/\rho$  where  $\phi$  is an eigenvalue of the transfer operator  $\mathcal{L}$  defined with respect to Lebesgue measure  $m$ . For systems which involve regions of low density with  $\rho$  close to zero, this is intractable to do numerically.

**7. Discussion and outlook.** We have used the transfer operator and the Koopman operator to disentangle the multiple slow and fast scales and provide an effective set of slow variables which can then be efficiently numerically integrated in time. We constructed a projection onto a slow subspace using the eigenfunctions of the Koopman operator. We then devised an algorithm to estimate the drift and diffusion terms of an assumed stochastic differential equation describing the reduced slow dynamics. This constitutes a huge computational advantage as we were able to use time steps of the order of  $10^4$  larger to propagate forward the slow variables when compared to the full multiscale system.

It is pertinent to mention that our approach defines the slow dynamics only up to a homeomorphism. Therefore our approach is not able to define a unique set of slow variables. One may, however, apply in a post processing procedure a coordinate transformation to the fast fibers which renders them straight along certain coordinate axes of the physical coordinates as for example in Figure 4.3. This would identify a set of physical coordinates as slow, but again, this transformation would not be unique as one could choose any smooth curve which is transverse to the fast fibers to be used to anchor fibers to slow variables  $v$ .

We now discuss several extension of the approach introduced in this work which are planned for future research.

**Extension to systems with multi-dimensional slow subspace:** In this paper, we considered multiscale examples with one-dimensional slow dynamics, so that the mapping  $\mathcal{P} : \mathcal{Z} \rightarrow \mathcal{X}$  could be approximated by a single eigenfunction  $\phi : \mathcal{Z} \rightarrow \mathbb{R}$  of the Koopman operator. We outline now how to extend our computational method to the case of a higher-dimensional slow subspace. Details are planned for further research. For a system with higher-dimensional slow dynamics, it will be necessary to approximate  $\mathcal{P}$  by a product of eigenfunctions

$$\mathcal{P} = \phi_1 \times \phi_2 \times \cdots \times \phi_m : \mathcal{Z} \rightarrow \mathbb{R}^m.$$

Then, a value  $v \in \mathbb{R}^m$  defines a fiber  $F = \mathcal{P}^{-1}(\{v\}) \subset \mathcal{Z}$ . The fiber dynamics can be defined as  $\hat{T} : F \rightarrow F$  where  $\hat{T} = \pi \circ T$  and  $\pi : U \rightarrow F$  is a mapping from a neighbourhood  $U$  down to the fiber itself. As explained in Section 6, for a single eigenfunction  $\phi$  the numerical computation of  $\pi(z)$  was given by the intersection of  $F$  with the line through  $z$  tangent to  $\nabla\phi(z)$ . To extend this to the general setting, define  $\pi(z)$  as the intersection of  $F$  with the  $m$ -dimensional plane through  $z$  spanned by the vectors  $\nabla\phi_i(z)$  for  $i = 1, \dots, m$ . As in Section 4.3.2, one can test the validity of the fiber dynamics by comparing the distance  $\|\hat{T}(z) - T(z)\|$  to the distance  $\|T(z) - z\|$  for an ensemble of points on  $F$ .

If the dimension of the slow dynamics is not known beforehand, an automated method to find the dimension is simply to test products of an increasing number of eigenfunctions until a product is found for which  $\hat{T}$  gives a reasonable approximation

of fast dynamics. Using this definition of  $\hat{T}$ , Algorithm 1 can be implemented exactly as before.

Algorithm 2 can also be generalized to a product of eigenvalues. In this case, for Step 3, each individual  $\phi_i$  is reparameterized to  $\theta_i$  as before, and  $\theta : \mathcal{Z} \rightarrow \mathbb{R}^m$  is defined as the product  $\theta = \theta_1 \times \cdots \times \theta_m$ . In Step 5c,  $\alpha_k(v)$  is computed as the  $m$ -dimensional mean of  $\{\theta(T^k(z_i)) - v\}_{i=1}^q$  and  $\beta_k(v)$  is computed as the  $m \times m$  covariance matrix of the ensemble. From this,  $\alpha$  and  $\beta$  in Steps 6 and 7 define a drift-diffusion process on  $\mathbb{R}^m$ .

**Extension to systems with more than two time scales:** In this paper, we considered dynamical systems with one fast and one slow time scale. We now present an iterative procedure using Algorithms 1 and 2 (or their higher-dimensional variants) which distills the dynamics on all different time scales. For ease of exposition we present this procedure for a system  $T$  with three time scales (fast, moderate and slow) which readily generalises. Applying Algorithm 1 to such a system produces fiber dynamics  $\hat{T} : F \rightarrow F$  which incorporates the dynamics of both the fast and moderate time scales. The slowest time scales can be obtained by applying Algorithm 2 to  $T$ . To further isolate the moderate and fast dynamics, apply Algorithms 1 and 2 now to the fiber dynamics  $\hat{T}$  in place of the full system  $T$ .

**Solving for the slow variables without ever having to integrate forward in time the fast variables:** We defined the projection to the slow subspace via the eigenfunctions of the Koopman operator. This requires the integration in time of the full dynamics, including the fast variables, needed for Ulam's method. Noting that the transfer operator  $\mathcal{L}$  and the infinitesimal generator  $\mathcal{A}$  share the same eigenfunctions, one can determine the generator simply by evaluating the vector fields without ever having to integrate forward in time the system [39].

**Acknowledgments.** The illustrations in Figures 2.1 and 5.1 were produced using the Asymptote vector-graphics language (<http://asymptote.sf.net>).

#### REFERENCES

- [1] V. ARNOLD, V.V. KOZLOV, AND A.I. NEISHTADT, *Mathematical Aspects of Classical and Celestial Mechanics*, Springer-Verlag, New York, 1993.
- [2] I. BABUŠKA AND J. E. OSBORN, *Finite element-Galerkin approximation of the eigenvalues and eigenvectors of selfadjoint problems*, Math. Comp., 52 (1989), pp. 275–297.
- [3] V. BALADI AND L.-S. YOUNG, *On the spectra of randomly perturbed expanding maps*, Comm. Math. Phys., 156 (1993), pp. 355–385.
- [4] NILS BERGLUND AND BARBARA GENTZ, *Noise-Induced Phenomena in Slow-Fast Dynamical Systems*, Springer, 2005.
- [5] MICHAEL BLANK, GERHARD KELLER, AND CARLANGLO LIVERANI, *Ruelle-Perron-Frobenius spectrum for Anosov maps*, Nonlinearity, 15 (2002), pp. 1905–1973.
- [6] CHRIS BOSE AND GARY FROYLAND, *Strange eigenmodes for invertible measure-preserving systems*. in preparation.
- [7] PETRA BOXLER, *A stochastic version of the centre manifold theorem*, Probab. Th. Rel. Fields, 83 (1989), pp. 509–545.
- [8] JOHN P. BOYD, *Chebyshev and Fourier spectral methods*, Dover Publications Inc., Mineola, NY, second ed., 2001.
- [9] J. CARR, *Applications of Centre Manifold Theory*, no. 35 in Applied Mathematical Sciences, Springer, 1981.
- [10] A.J. CHORIN AND O.H. HALD, *Stochastic Tools in Mathematics and Science*, STAMS, Springer-Verlag, New York, 2006.
- [11] A.J. CHORIN, O.H. HALD, AND R. KUPFERMAN, *Optimal prediction and the Mori-Zwanzig representation of irreversible processes*, Proceedings of the National Academy of Science, 97 (2000), p. 29682973.

- [12] R. COIFMAN, I. KEVREKIDIS, S. LAFON, M. MAGGIONI, , AND B. NADLER, *Diffusion maps, reduction coordinates and low dimensional representation of stochastic systems*, SIAM Multiscale Modeling and Simulation, 7 (2008), pp. 842–864.
- [13] R. COIFMAN AND S. LAFON, *Diffusion maps*, Applied and Computational Harmonic Analysis, 21 (2006), pp. 5–30.
- [14] MICHAEL DELLNITZ, GARY FROYLAND, AND STEFAN SERTL, *A conjecture on the existence of isolated eigenvalues of the Perron-Frobenius operator*, in International Conference on Differential Equations, Vol. 1, 2 (Berlin, 1999), World Sci. Publ., River Edge, NJ, 2000, pp. 1030–1032.
- [15] MICHAEL DELLNITZ AND OLIVER JUNGE, *On the approximation of complicated dynamical behavior*, SIAM J. Numer. Anal., 36 (1999), pp. 491–515.
- [16] M. DELLNITZ AND O. JUNGE, *On the approximation of complicated dynamical behaviour*, SIAM J. Numer. Anal., 36 (1999), pp. 491–515.
- [17] P. DEUFLHARD, W. HUISINGA, A. FISCHER, , AND C. SCHÜTTE, *Identification of almost invariant aggregates in nearly uncoupled Markov chains*, SIAM J. Numer. Anal., 315 (2000), p. 3959.
- [18] P. DEUFLHARD AND C. SCHÜTTE, *Molecular conformation dynamics and computational drug design*, in Applied Mathematics Entering the 21th Century, J. M. Hill and R. Moore, eds., ICIAM 2003, Sydney, 2004.
- [19] WEINAN E, *Analysis of the heterogeneous multiscale method for ordinary differential equations*, Comm. Math. Sci., 1 (2003), pp. 423–436.
- [20] WEINAN E, BJÖRN ENNGUIST, X. LI, W. REN, AND ERIC VANDEN-EIJNDEN, *Heterogeneous multiscale methods: A review*, Comm. Comp. Phys., 2 (2007), pp. 367–450.
- [21] GARY FROYLAND, *Computer-assisted bounds for the rate of decay of correlations*, Comm. Math. Phys., 189 (1997), pp. 237–257.
- [22] G. FROYLAND, *Statistically optimal almost-invariant sets*, Physica D, 200 (2005), p. 205219.
- [23] GARY FROYLAND, *On Ulam approximation of the isolated spectrum and eigenfunctions of hyperbolic maps*, Discrete Contin. Dyn. Syst., 17 (2007), pp. 671–689 (electronic).
- [24] GARY FROYLAND, OLIVER JUNGE, AND PÉTER KOLTAI, *Estimating long-term behavior of flows without trajectory integration: the infinitesimal generator approach*, SIAM J. Numer. Anal., 51 (2013), pp. 223–247.
- [25] GARY FROYLAND AND KATHRIN PADBERG, *Almost-invariant sets and invariant manifolds—connecting probabilistic and geometric descriptions of coherent structures in flows*, Phys. D, 238 (2009), pp. 1507–1523.
- [26] G. FROYLAND, K. PADBERG, M. ENGLAND, , AND A.M. TREGUIER, *Detection of coherent oceanic structures via transfer operators*, Physical Review Letters, 98 (2007), p. 224503.
- [27] G. FROYLAND, N. SANTITISSADEEKORN, AND A. MONAHAN, *Transport in time-dependent dynamical systems: Finite-time coherent sets*, Chaos, 20 (2010), p. 043116.
- [28] C. W GARDINER, *Handbook of Stochastic Methods for Physics, Chemistry, and the Natural Sciences*, Springer, New York, 3rd ed., 2003.
- [29] B. GAVEAU AND L. S. SCHULMAN, *Multiple phases in stochastic dynamics: Geometry and probabilities.*, Physical Review E, 73 (2006), p. 036124.
- [30] C.W. GEAR AND I. KEVREKIDIS, *Projective methods for differential equations*, SIAM J. Sci. Comp., 24 (2003), pp. 1091–1106.
- [31] DROR GIVON, RAZ KUPFERMAN, AND ANDREW STUART, *Extracting macroscopic dynamics: model problems and algorithms*, Nonlinearity, 17 (2004), pp. R55–R127.
- [32] G. A. GOTTWALD AND J. HARLIM, *The role of additive and multiplicative noise in filtering complex dynamical systems*, Proc. Roy. Soc. A, 469 (2013), p. 20130096.
- [33] GEORG A. GOTTWALD AND IAN MELBOURNE, *Homogenization for deterministic maps and multiplicative noise*, Proceedings of the Royal Society A: Mathematical, Physical and Engineering Science, 469 (2013).
- [34] W. JUST, H. KANTZ, C. RÖDENBECK, AND M. HELM, *Stochastic modelling: replacing fast degrees of freedom by noise*, J. Phys. A, 34 (2001), pp. 3199–3213.
- [35] I. KEVREKIDIS AND G. SAMAËY, *Equation-free multiscale computation: algorithms and applications*, Ann. Rev. Phys. Chem., 60 (2009), pp. 321–344.
- [36] I. G KEVREKIDIS, C. W. GEAR, J. M. HYMAN, G. K. PANAGIOTIS, O. RUNBORG, AND C. THEODOROPoulos, *Equation-free, coarse-grained multiscale computation: Enabling microscopic simulators to perform system-level analysis*, Comm. Math. Sci., 1 (2003), pp. 715–762.
- [37] R. Z. KHASMINSKY, *On stochastic processes defined by differential equations with a small parameter*, Theory of Probability and its Applications, 11 (1966), pp. 211–228.
- [38] P. E. KLOEDEN AND E. PLATEN, *Numerical methods for stochastic differential equations*, in

- Nonlinear dynamics and stochastic mechanics, CRC Math. Model. Ser., CRC, Boca Raton, FL, 1995, pp. 437–461.
- [39] P. KOLTAI, *Efficient approximation methods for the global long-term behavior of dynamical systems - Theory, algorithms and examples*, PhD thesis, Technische Universität München, 2010.
- [40] T. G. KURTZ, *A limit theorem for perturbed operator semigroups with applications to random evolutions*, Journal of Functional Analysis, 12 (1973), pp. 55–67.
- [41] TIEN YIEN LI, *Finite approximation for the Frobenius-Perron operator. A solution to Ulam’s conjecture*, J. Approximation Theory, 17 (1976), pp. 177–186.
- [42] H. W. LILLIEFORS AND C. C. MCBRIDE, *Kolmogorov-Smirnov and Anderson-Darling statistics with parameters estimated by linear combinations of order statistics and some robustness properties*, in Goodness-of-fit (Debrecen, 1984), vol. 45 of Colloq. Math. Soc. János Bolyai, North-Holland, Amsterdam, 1987, pp. 369–376.
- [43] W. LIU AND G. HALLER, *Strange eigenmodes and decay of variance in the mixing of diffusive tracers*, Physica D, 188 (2004), pp. 1–39.
- [44] J. MACLEAN AND G. A. GOTTWALD, *On convergence of the projective integration method for stiff ordinary differential equations*, Communications in Mathematical Sciences, 12 (2014), pp. 235–255.
- [45] ANDREW J. MAJDA, ILYA TIMOFEYEV, AND ERIC VANDEN EIJNDEN, *A mathematical framework for stochastic climate models*, Communications on Pure and Applied Mathematics, 54 (2001), pp. 891–974.
- [46] MATLAB, *version 7.10.0 (R2010a)*, The MathWorks Inc., Natick, Massachusetts, 2010.
- [47] IAN MELBOURNE AND ANDREW STUART, *A note on diffusion limits of chaotic skew-product flows*, Nonlinearity, 24 (2011), pp. 1361–1367.
- [48] IGOR MEZIĆ, *Spectral properties of dynamical systems, model reduction and decompositions*, Nonlinear Dynam., 41 (2005), pp. 309–325.
- [49] ———, *Analysis of fluid flows via spectral properties of the Koopman operator*, in Annual review of fluid mechanics. Volume 45, 2013, vol. 45 of Annu. Rev. Fluid Mech., Annual Reviews, Palo Alto, CA, 2013, pp. 357–378.
- [50] IGOR MEZIĆ AND ANDRZEJ BANASZUK, *Comparison of systems with complex behavior*, Phys. D, 197 (2004), pp. 101–133.
- [51] L. MITCHELL AND G. A. GOTTWALD, *Data assimilation in slow-fast systems using homogenized climate models*, Journal of the Atmospheric Sciences, 69 (2012), pp. 1359–1377.
- [52] H. MORI, H. FUJISAKA, AND H. SHIGEMATSU, *A new expansion of the master equation*, Prog. Theor. Phys., 51 (1974), pp. 109–122.
- [53] N. NAMACHCHIVAYA AND G. LENG, *Equivalence of stochastic averaging and stochastic normal forms*, J. Appl. Mech., 57 (1990), pp. 1011–1017.
- [54] N. NAMACHCHIVAYA AND Y.K. LIN, *Method of stochastic normal forms*, Int. J. Non-Linear Mechanics, 26 (1991), pp. 1011–1017.
- [55] T. N. PALMER, *A nonlinear dynamical perspective on climate prediction*, J. Climate, 12 (1999), pp. 575–591.
- [56] G. C. PAPANICOLAOU, *Some probabilistic problems and methods in singular perturbations*, Rocky Mountain Journal of Mathematics, 6 (1976), pp. 653–674.
- [57] GRIGORIS A. PAVLIOTIS AND ANDREW M. STUART, *Multiscale Methods: Averaging and Homogenization*, Springer, New York, 2008.
- [58] ANTHONY J. ROBERTS, *Normal form transforms separate slow and fast modes in stochastic dynamical systems*, Physica A, 387 (2008), pp. 12–38.
- [59] J.A. SANDERS AND F. VERHULST, *Averaging methods in nonlinear dynamical systems*, vol. 59 of Applied Mathematical Sciences, Springer-Verlag, New York, 1985.
- [60] C. SCHÜTTE, W. HUISINGA, AND P. DEUFLHARD, *Transfer operator approach to conformational dynamics in biomolecular systems*, in Ergodic Theory, Analysis, and Efficient Simulation of Dynamical Systems, B. Fiedler, ed., Springer, Berlin, 2001, pp. 191–223.
- [61] PETER SJÖGREN, *Operators associated with the Hermite semigroup—a survey*, in Proceedings of the conference dedicated to Professor Miguel de Guzmán (El Escorial, 1996), vol. 3, 1997, pp. 813–823.
- [62] P. STINIS, *Higher order Mori-Zwanzig models for the Euler equations*, SIAM Multiscale Modeling and Simulation, 6 (2007), pp. 741–760.
- [63] S. M. ULAM, *A collection of mathematical problems*, Interscience Tracts in Pure and Applied Mathematics, no. 8, Interscience Publishers, New York-London, 1960.
- [64] J. WALTER AND C. SCHÜTTE, *Conditional averaging for diffusive fast-slow systems: A sketch for derivation*, in Analysis, Modeling and Simulation of Multiscale Problems, A. Mielke, ed., Springer, Berlin, 2006, pp. 647–682.

- [65] R. ZWANZIG, *Ensemble method in the theory of irreversibility*, J. Chem. Phys., 33 (1960), pp. 1338–1341.
- [66] ROBERT ZWANZIG, *Nonequilibrium Statistical Mechanics*, Oxford University Press, Oxford, 2001.